AD A124637

ASSESSMENT OF
SURFACE WAVE EFFECTS
ON UPPER OCEAN PARAMETERS

MARINE ENVIRONMENTS CORPORATION

12

ASSESSMENT OF

SURFACE WAVE EFFECTS

ON UPPER OCEAN PARAMETERS

Prepared for:

Ocean Measurements Program
Naval Ocean Research and Development Activity
NSTL Station, Mississippi 39529

Prepared by:

Marshall D. Earle
Marine Environments Corporation
10629 Crestwood Drive
Manassas, Virginia 22110

January 1983

Report MEC-13-W

UNCLASSIFIED

SECURITY CLASSIFICATION OF THIS PAGE (When Data Entered)

REPORT DOCUMENTATION PAGE		READ INSTRUCTIONS BEFORE COMPLETING FORM
1. REPORT NUMBER MEC-13-W	2. GOVT ACCESSION NO. AD-A124637	3. RECIPIENT'S CATALOG NUMBER
4. TITLE (and Subtitle) ASSESSMENT OF SURFACE WAVE EFFECTS ON UPPER OCEAN PARAMETERS		5. TYPE OF REPORT & PERIOD COVERED Final Report 3/82-1/83
		6. PERFORMING ORG. REPORT NUMBER MEC-13-W
7. AUTHOR(s) Marshall D. Earle		8. CONTRACT OR GRANT NUMBER(s) N00014-82-C-0237
9. PERFORMING ORGANIZATION NAME AND ADDRESS Marine Environments Corporation 10629 Crestwood Drive Manassas, Virginia 22110		10. PROGRAM ELEMENT, PROJECT, TASK AREA & WORK UNIT NUMBERS
11. CONTROLLING OFFICE NAME AND ADDRESS Naval Ocean Research and Development Activity, NORDA Code 540 NSTL Station, Mississippi 39529		12. REPORT DATE January 1983
		13. NUMBER OF PAGES 86
14. MONITORING AGENCY NAME & ADDRESS(if different from Controlling Office)		15. SECURITY CLASS. (of this report) UNCLASSIFIED
		15a. DECLASSIFICATION/DOWNGRADING SCHEDULE

16. DISTRIBUTION STATEMENT (of this Report)

Unlimited

17. DISTRIBUTION STATEMENT (of the abstract entered in Block 20, if different from Report)

Unlimited

18. SUPPLEMENTARY NOTES

19. KEY WORDS (Continue on reverse side if necessary and identify by block number)

Ocean waves, ocean surface waves, inertial currents, internal waves, wave breaking, wave mixing

20. ABSTRACT (Continue on reverse side if necessary and identify by block number)

See next page.

DD FORM 1 JAN 73 1473 EDITION OF 1 NOV 65 IS OBSOLETE
S/N 0102-LF-014-6601

UNCLASSIFIED
SECURITY CLASSIFICATION OF THIS PAGE (When Data Entered)

Effects of surface waves on upper ocean physical oceanographic parameters of interest to the Ocean Measurements program (OMP) are investigated. Three surface wave effects are potentially important to the OMP. These are: generation of inertial currents and associated vertical shear, generation of high frequency internal waves within the seasonal thermocline, and increased mixing and decreased vertical gradients near the surface due to wave breaking and wave maintenance of turbulence.

Theory relating to each of these effects is provided and mathematical calculations are made which indicate the potential importance of these effects for the OMP. These effects increase with wind speed and sea state and are thus potentially important in mid-to-high latitude regions. These regions have relatively high wind speeds and wave heights due to prevailing westerly winds and the presence of primary extratropical storm tracks. Surface wave effects are largest near the surface and may be significant for depths less than approximately 100 meters.

No measurements have been previously interpreted in a manner to quantitatively determine the importance of these surface wave effects in the actual ocean. Such interpretation is needed because these effects are second order effects in terms of wave theory and existing theoretical approaches involve simplifying assumptions. Without suitable data interpretation, no theoretical or modeling technique can be judged suitable for routine operational use. Wave effects may be implicitly, but incorrectly, considered in present upper ocean models and data interpretations with wind dependence. This situation occurs because surface wave effects increase with sea state which increases with wind speed. However, the intermediate role of waves between the wind and upper ocean features changes the form of wind speed dependence so that improved results might be obtained by consideration of wave effects. Characteristics of several existing upper ocean data sets are consistent with the presence of surface wave effects and consideration of wave effects might lead to different interpretations than have been reported for these data sets. A shortcoming of existing data sets is that the measurements were not planned to evaluate surface wave effects so that information for detailed analysis may not be available.

Since the importance of surface wave effects has not been proven from measurements, emphasis should be placed on supplemental development of wave information, including measurements and hindcasts, during future upper ocean field experiments to provide data sets suitable for further analysis of wave effects. Guidance is provided for development of needed wave information.

TABLE OF CONTENTS

FIGURE LIST

TABLE LIST

1. INTRODUCTION

The Ocean Measurements Program (OMP) is concerned with measurements and modeling of upper ocean physical oceanographic parameters such as current shear, temperature, and salinity. Of these parameters, current shear is most important. Until now, the OMP has not considered surface waves in planning or interpretation of upper ocean measurements and the development of upper ocean models. Surface waves are defined here as wind-driven gravity waves. Primary geographical regions of interest to the OMP are mid-latitudes to high latitudes in the Northern Hemisphere. Primary tracks of extratropical storms are within these regions so that surface waves with heights of several to many feet are a common occurrence and very high wave heights are not unusual. From a wave theory point of view, potential wave effects of concern to the OMP are second order effects which become more important for higher wave heights such as those which occur in the regions of interest.

This report describes potential surface wave effects on:

-- Current shear due to inertial currents,

-- Generation of upper ocean internal waves, and

-- Vertical distributions of shear and other parameters such as temperature and salinity.

The strongest emphasis is on current shear and the least emphasis is on vertical distributions of other parameters. These distributions are affected primarily by increased eddy coefficients near the surface due to surface waves. Capability of waves to increase

eddy coefficients is described.

This report is a review of scientific literature providing information from which surface wave effects are assessed. Available scientific work pertinent to this assessment is limited by the lack of unified work, particularly interpretation of measurements, involving both surface waves and internal ocean parameters such as inertial currents and internal waves. Oceanographers who interpret ocean current data seldom work in the area of ocean surface waves, and oceanographers who interpret ocean surface wave data seldom work in the area of ocean currents. As a result, the available scientific work for this assessment tends to be highly specialized with inadequate observational interpretations to verify or improve available theories . Because simplifying assumptions are often needed to make theoretical solutions mathematically tractable, it is possible that practical applications may require use of numerical approaches to consider surface wave effects. In addition, there are very little measured data that are adequate to test the theories or to provide the basis for better theories. A serious practical problem is the difficulty of making measurements near the surface in the presence of waves particularly for higher wave conditions when surface wave effects become more important. The Oceanographic Instrumentation Systems (OIS) part of the OMP is sponsoring development of instrumentation for measurement of upper ocean parameters such as current shear. If coupled with capability to routinely and simultaneously measure surface wave conditions, this instrumentation could provide the data necessary to more quantitatively evaluate the wave effects described here.

The following sections describe potential surface wave effects. In order to provide a physical understanding of these effects, which is necessary for planning measurement and modeling projects that may further examine these effects, a summary of the basic theory for each effect is provided. Use of basic theory is also necessary to make

quantitative calculations from mathematical equations. The report shows the potential importance of surface wave effects in regions with high wind speeds and provides guidance for OMP measurements to further evaluate surface wave effects. A bibliography of all references that were found useful is included for use by the OMP and OMP principal investigators. The report does not analyze potential wave effects on measurements by particular sensors under development through OMP sponsorship.

2. INERTIAL CURRENTS

A. INTRODUCTION

When wind blows over the sea surface, momentum is transferred to the ocean producing both wind waves and wind-driven currents. Theoretical treatment of wind-driven currents has, for the most part, separately considered direct current generation by tangential wind stress and surface wave-induced current generation. The classical Ekman (1905) model, in which wind-driven currents are generated from a balance between tangential surface wind stress and Coriolis force neglecting surface wind waves, and models such as those of Bye (1967) and Kenyon (1969), in which currents are assumed to be the result of a Stokes current derived from the local wave field, are examples of such treatments. Stokes current models are irrotational and neglect tangential surface wind stress. It is apparent that models using only tangential wind stress and models using only Stokes currents can only approximate the physics of the actual situation.

Addition of surface wave effects in surface current models has been attempted by Korvin-Krovkovsky (1972), Ianneillo and Garvine (1975) and Bishop (1979). In each of these studies, uncoupled models were proposed in which total drift was calculated as the sum of Stokes plus Ekman currents. In only the last of these three was the influence of the Coriolis forces on Stokes drift and the subsequent coupling of the Stokes and Ekman currents considered in an ad hoc fashion. Huang (1979), using the work of Craik and Leibovich (1976) and Leibovich (1977), developed a coupled Stokes-Ekman wind-driven current model that includes effects of Coriolis force. Huang employed the conventional Eulerian description of surface water movement and included Stokes currents using a perturbation technique suggested by Leibovich (1977). The result was a model that includes the combined effects of wind stress and surface waves on current flow. The

model also gives a framework with which both Langmuir circulation and current flow can be considered jointly. However, the resulting mathematics is highly nonlinear and cannot be easily applied to practical problems. Madsen (1978) used the Lagrangian equations of motion to develop another coupled wind and surface wave current model. Huang (1982) pointed out several shortcomings in this analysis. First, Madsen's assumption that currents were independent of horizontal position ruled out Langmuir circulation. Without Langmuir circulation, the Madsen model is essentially of the Ekman type and predicts surface currents at approximately 37° to 45° to the right of the wind in the Northern Hemisphere. Observed surface current angles from the wind direction are usually much smaller often being closer to 20° (e.g. Bishop, 1979). Additionally, the eddy viscosity form used by Madsen was criticized because it is dimensionally incorrect.

Hasselmann (1970) has shown, using a theory first presented by Ursell (1950), that once a wave-induced Stokes current is established it cannot remain irrotational since the Coriolis force causes rotation in such a manner that the original Stokes momentum is transferred to an inertial oscillation. Since inertial currents are a common feature of upper ocean current measurements and make important contributions to vertical shear, generation of inertial currents through Coriolis force action on wave-caused Stokes currents is of particular interest.

The following sections review the theory of Stokes currents, note their magnitudes, and describe their role in the generation of inertial currents.

B. THEORY OF STOKES CURRENTS PRODUCED BY SURFACE WAVES

While Stokes currents associated with waves have been known since the middle of the last century (Stokes, 1847), only recently has the importance of these currents on other oceanic phenomena begun to be investigated in detail (e.g., Longuet-Higgins, 1969). Longuet-Higgins called attention to the difference between the mean current at a fixed point, known as the Eulerian mean current, and the mean current following a fluid particle which passes this point, known as the Lagrangian mean current. The difference in these mean values is the Stokes current. The following formulation applies:

$$V_L = V_E + V_S \tag{2.1}$$

where

V_L = Lagrangian mean current,
V_E = Eulerian mean current, and
V_S = Stokes current.

Following Longuet-Higgins (1969), assume that the velocity vector, $\vec{V}$, is fluctuating periodically with time. Define, $\vec{V}$, in the Eulerian system of coordinates $\vec{x} = (x, y, z)$ fixed in space. The time-averaged velocity, $\langle\vec{V}\rangle$, is small compared to $\vec{V}$ but not zero. When a marked parcel with initial position, $\vec{x}_o$, as shown in Figure 2.1, at time t_o moves to a new position $\vec{x}_o+\vec{\Delta x}$ at time t, its velocity at the new position is not equal to the velocity at $\vec{x}_o$ but to a different velocity

$$\vec{V}(\vec{x}, t) = \vec{V}(\vec{x}_o, t) + \Delta\vec{x}\cdot\nabla\vec{V}(\vec{x}_o, t) \tag{2.2}$$

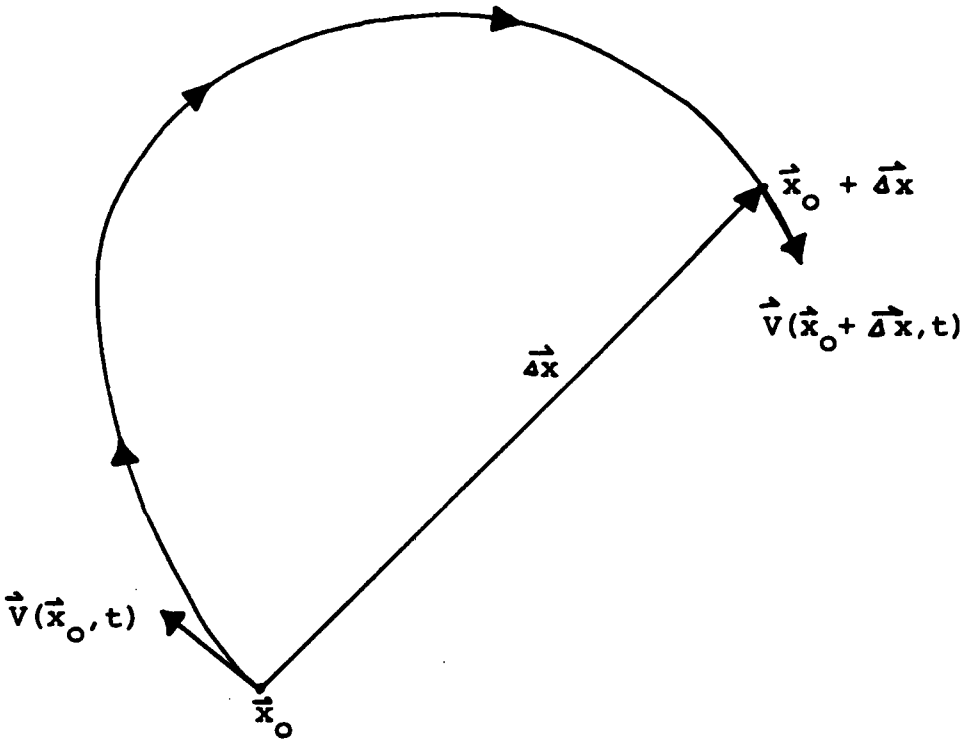

FIGURE 2.1. Trajectory of a Marked Fluid Parcel Moving from an Initial Position, $\vec{x}_o$, to a Final Position, $\vec{x}_o + \vec{\Delta x}$, where the Velocity is Spatially Changing (after Longuet-Higgins, 1969).

which depends on the spatial change of the velocity field.

Equation (2.2) is correct to order $\vec{\Delta x}$, quantities of higher order having been neglected. If the parcel oscillates in the neighborhood of its initial position in such a manner that $\vec{\Delta x}$ is small compared to the local length scale of the velocity field, then

$$\vec{\Delta x} = \int_{t_o}^{t} \vec{V}(\vec{x}_o, t)\ dt \tag{2.3}$$

to the same order of approximation. Substituting Equation (2.3) into Equation (2.2) and taking mean values over many wave cycles gives

$$\langle \vec{V}(\vec{x}, t) \rangle = \langle \vec{V}(\vec{x}_o, t) \rangle + \left\langle \int \vec{V}(\vec{x}_o, t)\, dt \cdot \nabla \vec{V}(\vec{x}_o, t) \right\rangle \tag{2.4}$$

with the following definitions

$$V_L = \langle \vec{V}(\vec{x}, t) \rangle \tag{2.5}$$

$$V_E = \langle \vec{V}(\vec{x}_o, t) \rangle \tag{2.6}$$

The third term, the difference between V_L and V_E, is given by

$$V_S = \left\langle \int \vec{V}(\vec{x}_o, t)\, dt \cdot \nabla \vec{V}(\vec{x}_o, t) \right\rangle \tag{2.7}$$

and is called the Stokes velocity. Hence, as in Equation (2.1)

$$V_L = V_E + V_S \tag{2.8}$$

Stokes currents produced by surface waves can be explained in simple terms by the difference between the faster forward velocity beneath a wave crest and the lower backward velocity beneath a wave trough. Decay of wave orbital velocity with depth causes a spatial gradient to occur in the velocity field so that water parcels move at different velocities in various parts of the velocity field. Stokes currents arise when currents are averaged in a spatially changing velocity field with an averaging interval which is longer than the period of oscillation.

To illustrate how Stokes currents are calculated, consider a single deep water sinusoidal surface wave component propagating in the positive x direction and with orbital velocity components in the horizontal and vertical directions given by

$$V_x = a\sigma \exp(kz)\cos(kx-\sigma t) \tag{2.9}$$

$$V_z = a\sigma \exp(kz)\sin(kx-\sigma t) \tag{2.10}$$

where

a = wave amplitude,

σ = wave radian frequency ($\sigma^2 = gk$),

g = acceleration due to gravity,

k = wave number,

z = vertical coordinate (0 at the sea surface and positive upward),

x = horizontal coordinate, and

t = time.

Use of these velocity components in Equation (2.7) yields the Stokes current which is given by

$$V_S = (a\sigma)(ak)\exp(2kz) \tag{2.11}$$

The factor (ak) is proportional to wave slope. Compared to the Eulerian velocity, i.e. equations (2.9) and (2.10), the Stokes current is considered a second order effect in terms of wave slope. A typical value of ak is 0.1 and waves break at maximum ak values approximately equal to 0.5. With depth, Stokes currents decrease twice as rapidly as orbital velocities.

The sea surface can be statistically considered as a superposition of numerous wave components with different amplitudes, frequencies, directions, and phases (which are randomly distributed over 0 to 2π). A wave directional spectrum provides the distribution of wave variance (proportional to wave amplitude squared and to wave energy) as a function of frequency and direction. The contribution to the variance in the frequency range (σ, $\sigma+d\sigma$) and direction range (Θ, $\Theta+d\Theta$) is given by

$$E(\sigma,\Theta)\,d\sigma\,d\Theta \tag{2.12}$$

where $E(\sigma,\Theta)$ is a spectral energy density. A directional spectrum can also be written as a wave number spectrum which provides the distribution of wave variance as either a function of wave number magnitude and direction or as a function of two horizontal wave number components. Integration of the directional spectrum, $E(\sigma,\Theta)$, over all directions provides the frequency spectrum, $E(\sigma)$. The Stokes current for waves propagating in a dominant direction with a frequency spectrum, $E(\sigma)$, is

$$V_S = \frac{2}{g} \int_0^\infty \sigma^3 \exp(2\sigma^2 z/g)\; E(\sigma)\,d\sigma \tag{2.13}$$

where the deep water surface wave dispersion relationship, $\sigma^2=gk$, is used. When waves cannot be considered to be almost unidirectional, an expression for the Stokes current within a directional band, $d\Theta$, is

$$V_S(\Theta) = \frac{2}{g} \left\{ \int_0^\infty \sigma^3 \exp(2\sigma^2 z/g) E(\sigma,\Theta)\,d\sigma \right\} d\Theta \tag{2.14}$$

C. STOKES CURRENT CALCULATIONS

Stokes currents for individual surface waves can be easily calculated by means of Equation (2.11). For example, a 1 m amplitude wave with a period of 6 seconds has a surface Stokes current of 12 cm-s^{-1}. A 5 m amplitude wave with a period of 10 seconds,

which might occur in storm conditions, has a surface Stokes current of 63 cm-s^{-1}. Of more interest, however, are Stokes currents generated by empirical wave spectra for given wind speeds. A Pierson-Moskowitz (1964) spectrum for fully-developed waves is given by

$$E_{PM}(\sigma) = \frac{\alpha g^2}{\sigma^5} \exp\left\{-\beta (\sigma_o/\sigma)^4\right\} \tag{2.15}$$

where $\alpha = 8.1\ 10^{-3}$, g is the acceleration due to gravity, $\beta = 0.74$, and $\sigma_o = g/u_{19.5}$ with $u_{19.5}$ being the wind at an elevation of 19.5 m above the sea surface. Substitution of Equation (2.15) into Equation (2.13) provides the Stokes current for fully-developed seas as a function of wind speed. Kenyon (1969) performed this calculation to show that the Stokes current at the surface is given by

$$V_{S(PM)} = 0.0157\ u_{19.5} \tag{2.16}$$

In other words, the surface Stokes current is 1.57% of the wind speed. Chang (1969) provided similar derivations for Stokes currents. Wind-driven surface currents, both from theory and observations, are typically considered to have speeds of 2% to 3% of the wind speed. Stokes currents may be approximately 50% of these values.

While seas are often not fully-developed, especially for higher wind speeds, this result shows that Stokes currents can be quite large, particularly in mid-to-upper latitudes near extratropical storm tracks. As an example, in January near 57°N, 26°W in the North Atlantic Ocean, 21% of wind speeds are greater than 34 knots (approximately 17 m-s^{-1})

and 8% of wind speeds are greater than 41 knots (approximately 20 $m\text{-}s^{-1}$) based on ship observations (Naval Weather Service Detachment, 1974). For these two cases, Stokes currents, based on fully-developed seas, are about 27 $cm\text{-}s^{-1}$ and 31 $cm\text{-}s^{-1}$. Numerous Lagrangian observations of surface water movement have indicated the possible presence of Stokes currents. For example, oil spill trajectories are often observed to move at an angle from the downwind direction that can only be obtained by consideration of Ekman wind generated currents combined with Stokes currents (e.g. Bishop, 1979). Such considerations can also explain movement of satellite tracked drifters in the North Pacific Ocean (Kirwan et al., 1979). While precise separation of Stokes currents and other currents is difficult, evidence shows that Stokes currents are important particularly in higher sea states.

Stokes currents decrease rapidly with depth due to the exponential decay factor in Equation (2.13). For fully-developed seas, depth attenuation becomes less with increasing wind speed because longer period waves are generated. Stokes currents become very small for depths greater than approximately one-fourth the wavelength corresponding to the frequency with maximum spectral wave energy. Thus, Stokes currents typically "penetrate" the ocean to a depth less than the wind-mixed layer. One implication of this situation was found by Kenyon (1970) who calculated that the Stokes current mass transport was only 16% to 32% of the Ekman mass transport for wind speeds of 10 to 20 $m\text{-}s^{-1}$.

A discrete numerical wave directional spectra model such as the one operated by the U.S. Navy provides wave variance within a discrete set of frequency and direction bands at grid points covering an oceanic region. Equation (2.14) can be directly used with the model ouput by replacing the integral with summations over the individual frequency bands and performing a separate summation for each direction band. Chin (1971) used

output from one of the earlier discrete numerical wave directional spectra models developed by Pierson and his co-workers (e.g. Baer, 1962; Pierson, Tick, and Baer, 1966) to calculate Stokes currents in the North Atlantic Ocean during parts of February and March, 1967. The Stokes currents for each direction band, twelve in this case, were vectorially summed to provide an estimate of the total Stokes drift.

D. INERTIAL CURRENTS PRODUCED BY STOKES CURRENTS

In the previous Stokes current formation, Coriolis force is not included. The orbital velocity components of the waves are thus in exact quadrature; that is, the horizontal and vertical wave orbital velocities are 90° out of phase. Accordingly there can be no wave induced Reynolds stress. In nature the earth's rotation induces a small perturbation that causes the circular particle orbits to be at a slight angle to the vertical. The resulting Reynolds stress generates a mean Eulerian current that turns out to be exactly equal and opposite to the original Stokes current. Hasselmann (1970) has shown how this mean Eulerian current provides the forcing for wave induced inertial oscillations. Consider the horizontal components of the equations of motion in which a Stokes current is present given as

$$\frac{\partial U_E}{\partial t} - fV_E = 0 \tag{2.17}$$

$$\frac{\partial V_E}{\partial t} + fU_E = -fU_S \tag{2.18}$$

where U_e is the x component and V_e is the y component of an Eulerian current and U_s

represents the Stokes current produced by surface waves on a rotating earth. The wind is blowing along on the x-axis so that the Stokes current is in the x direction. Define the complex Eulerian current as

$$W_E = U_E + iV_E \tag{2.19}$$

where $i^2 = -1$ so that the component equations may be written as

$$\frac{\partial W_E}{\partial t} + ifW_E = -ifU_S \tag{2.20}$$

The solution to this equation for an initial current, $W = W_o$ at $t = 0$, is an inertial oscillation of the form:

$$W_E = W_o\cos(ft) - iW_o\sin(ft) - U_S \tag{2.21}$$

The Langrangian current, W_L, is given by

$$W_L = W_o\cos(ft) - iW_o\sin(ft) \tag{2.22}$$

For the special case in which, $W_E = 0$ at $t = 0$,

$$W_E = U_S\cos(ft) - iU_S\sin(ft) - U_S \tag{2.23}$$

$$W_L = U_S\cos(ft) - iU_S\sin(ft) \tag{2.24}$$

Interpretation of these results illustrates development of inertial currents as a consequence of wave generated Stokes currents. Figure 2.2 is a polar representation of developing Eulerian and Lagrangian inertial currents generated by an existing Stokes current. Both the Eulerian and Lagrangian currents rotate clockwise (in the Northern Hemisphere). At $t = 0$, the Eulerian current is zero and the Lagrangian current equals the Stokes current. At $t = \pi/f$, the Eulerian current reaches a maximum value of twice the Stokes current and is in the opposite direction of the original Stokes current. At this time, the Lagrangian current is equal to the Stokes current but is also opposite to the direction of the original Stokes current. If the Stokes current remains constant, that is wave conditions remain constant, the oscillations repeat with frequency f. In other words, these are inertial oscillations. Two important features are that the Lagrangian inertial oscillations have zero mean value and the Eulerian inertial oscillations reach maximum values twice the magnitude of the Stokes current. In the last section, the Stokes current was shown to have appreciable values, especially for higher wind speeds, so that wave generated Eulerian inertial oscillations are expected to be important in the upper ocean.

In mid-to-upper latitudes, for example 45^{o} to 70^{o}, the inertial frequency, f, corresponds to periods between 13 and 17 hours. At lower latitudes, inertial periods are longer. Seldom are wind and wave conditions stationary over these time periods. Thus, the oscillations expressed by Equations (2.23) and (2.24) will not repeat for many cycles. If wave heights abruptly decrease so that the Stokes current effectively vanishes at a given time, the initial value of the inertial current depends on the time of the wave height decrease. If this time is $t = \pi/f$, a large inertial current equal to twice the Stokes current would exist. If this time is $t = 2\pi/f$, there would be no inertial current. The general

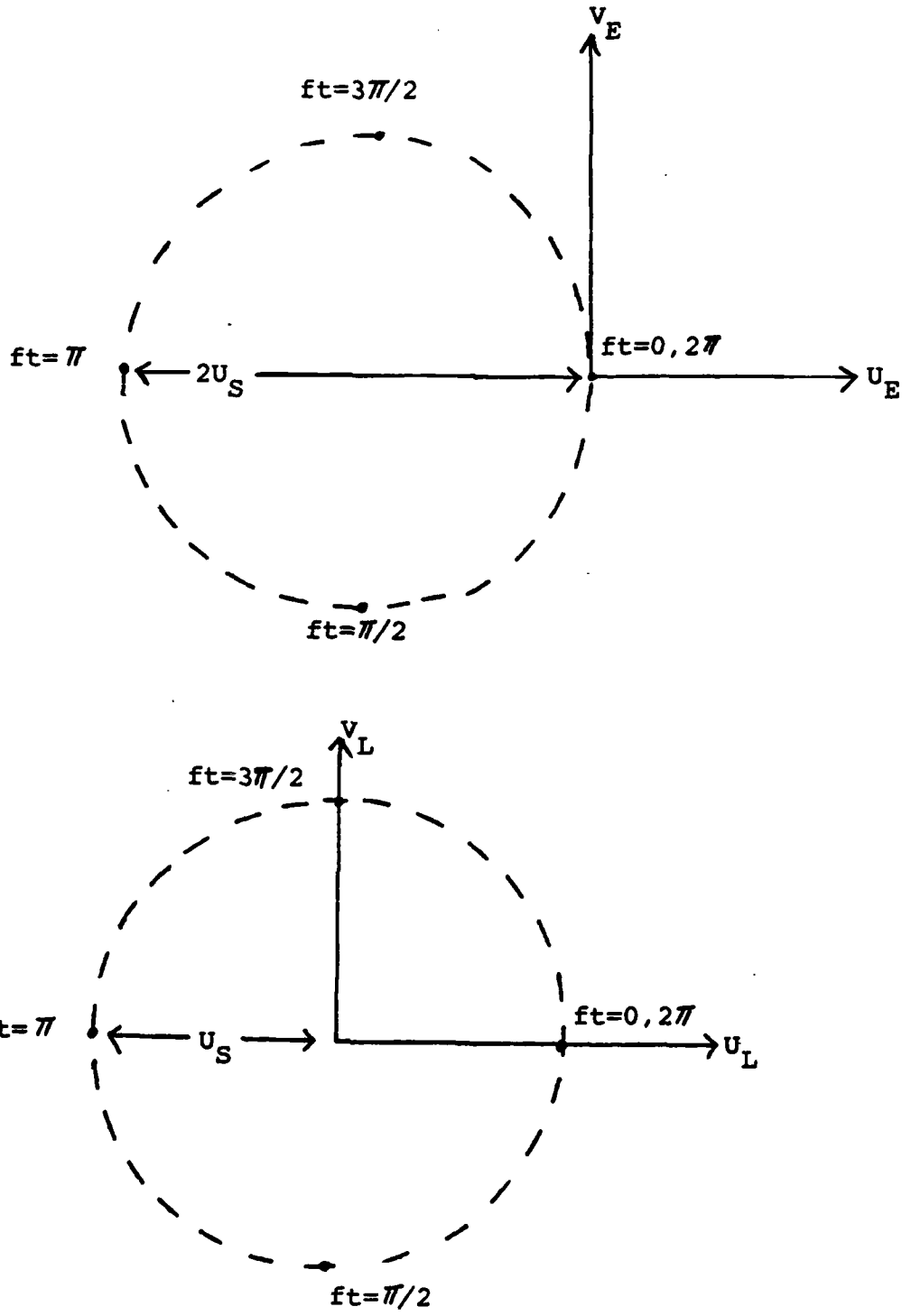

FIGURE 2.2. Polar Representation of Eulerian (Top) and Lagrangian (Bottom) Inertial Currents for an Existing Stokes Current, U_S.

solution to Equation (2.20) when the Stokes current varies slowly with time is given by Hasselmann (1970) as

$$W_E(t) = W_E(t=0) \mp if \int_0^t \exp(\mp if(t-t')) U_S(t') \, dt' \qquad (2.25)$$

Figure 2.3 is an example provided by Hasselmann for the special case where a constant Stokes current begins to decrease linearly with time at time $t = 5\pi/f$. For this case, the gradual cut-off of the Stokes current results in Eulerian inertial currents 1.64 as large as the Stokes current. As noted by Hasselmann, dependence of inertial current velocities on the timing of Stokes current fluctuations may account for variability of inertial currents generated by different storms with comparable strengths. In the actual ocean, Stokes currents can be expected to cause a considerable degree of randomness in local inertial currents.

In review, in a non-rotating system, ocean surface waves cannot produce a Reynolds stress and thus produce no direct Eulerian current. In this case

$$W_E = 0 \qquad (2.26)$$

and

$$W_L = W_E + U_S = U_S \qquad (2.27)$$

On the rotating earth the wave trajectories are still circles but they are tilted at a slight angle to the vertical. This produces a Reynolds stress proportional to, $-fU_S$, and a subsequent inertial current. The equation of motion thus takes the form

$$\frac{\partial W_E}{\partial t} + ifW_E = -ifU_S \qquad (2.28)$$

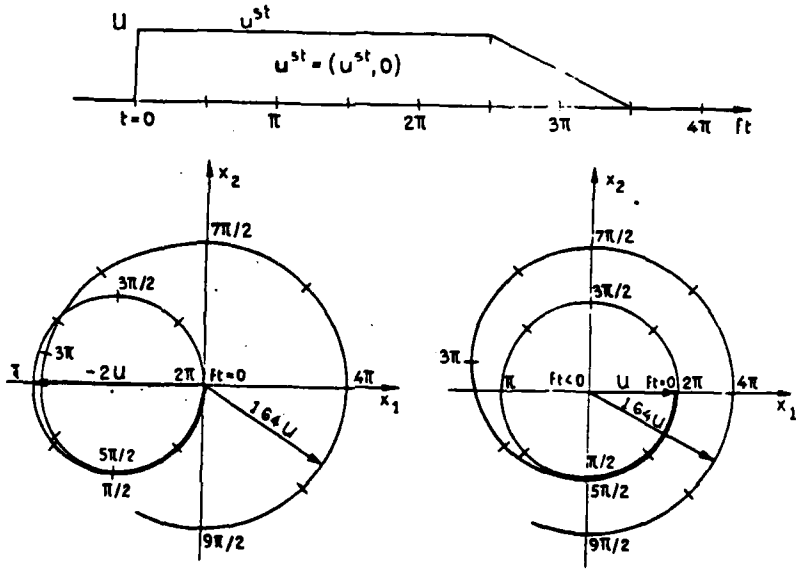

Eulerian Current Lagrangian Current

FIGURE 2.3. Polar Representation of Eulerian and Lagrangian Inertial Currents Generated by a Stokes Current U^{st} in the x_1 Direction Where the Stokes Current Begins to Linearly Decrease With Time at Time $ft=5\pi/2$ (from Hasselmann, 1970). After the Stokes current is no longer present, the Eulerian current has a value 1.64 as large as the Stokes current.

and the solution has the form

$$W_E = W_o\cos(ft) - iW_o\sin(ft) - U_S \tag{2.29}$$

$$W_L = W_o\cos(ft) - iW_o\sin(ft) \tag{2.30}$$

In the steady-state

$$ifW_E = -ifU_S \tag{2.31}$$

$$W_E = -U_S \tag{2.32}$$

and

$$W_L = W_E + U_S = 0 \tag{2.33}$$

so that the Lagrangian current vanishes.

In the transient case the transient Eulerian inertial current may have an amplification of up to twice the Stokes current value. This value is dependent on time variations of waves and Stokes currents relative to the inertial cycle. This may explain why storms of similar magnitude produce different inertial responses. As an example, Pollard and Millard (1970) provide time histories of wind velocity and near surface inertial currents. For two storm events (October 8, 1965, and October 17-18, 1965) with similar wind speeds of about 12 $m\text{-}s^{-1}$ (and hence similar Stokes currents of about 18 $cm\text{-}s^{-1}$) but with different durations, Equation (2.23) provides inertial currents differing by a factor of about 1.5 as seen in the measurements. These rough calculations are not conclusive but indicate that surface wave effects may be important for modeling inertial current response

to winds and thus inertial current contributions to vertical current shear.

Chin (1971) used the approach outlined here with Stokes currents calculated from a discrete numerical wave directional spectra model as noted in Section 2-C to produce time histories of surface wave generated inertial currents in the North Atlantic Ocean during February and March, 1967. The temporal variations of the calculated currents at given locations and their correlations with storm events is consistent with characteristics of observed inertial currents.

In the ocean, inertial currents have been observed to be damped with time. The model presented here does not account for this observed damping and this project does not address the damping or dissipation of inertial oscillations. Hasselmann (1970) notes that if either the wave field or the ocean are weakly nonhomogeneous, inertial oscillations disperse in both the vertical and horizontal directions due to a phase mixing process with closely neighboring frequencies. In a recent investigation for the OMP, Rubenstein (1982) briefly reviews several mechanisms for dissipation of inertial oscillations and shows that vertical dispersion may account for the observed rapid decay of inertial oscillations with depth. Whether inertial currents are generated "directly" by wind stress, "indirectly" by surface waves generated by wind stress, or by the likely combination of both processes, the same dissipation mechanisms should occur.

E. VERIFICATION BY MEASUREMENTS

The role of surface waves in generating inertial currents has not been verified by detailed examination of any data set. This is unfortunate because inertial currents, which decay with depth, are a common feature of upper ocean current measurements. Thus, inertial currents are expected to contribute substantially to vertical current shear. For

example in recent work for the OMP, Rubenstein and Newman (1982) analyzed data from a triangular array of moorings off the eastern U.S. continental slope (Woods Hole Site D, 39°N latitude, 70°W longitude) to determine vertical shear. Current shear spectra had strong peaks near the inertial frequency, 0.053 c.p.h. (period = 19 hours), especially when shear was computed from the uppermost current meters at depths of 12 and 32 m. Coherence between vertical shear and wind stress was statistically significant when shear was computed from the uppermost current meters but was not significant when shear was computed from somewhat deeper current meter pairs at depths of 32 and 52 m and at depths of 52 and 72 m. As noted by Rubenstein and Newman, this behavior is consistent with downward propagation of near-inertial oscillations that had been generated by wind stress at other times and locations. However, this behavior may also be consistent with portions of the near-inertial currents being generated by surface waves. Surface waves are not only a function of wind stress but also are a function of the spatial and temporal variation of the wind field (i.e. wind fetch and duration in wave terminology). In addition, surface waves at a given location may contain considerable contributions from winds at other locations. Surface waves may also propagate as swell at speeds greater than advection speeds of atmospheric systems that generated the waves. Finally, as indicated by Hasselmann (1970), the timing of Stokes drift time variations relative to inertial oscillations affects the magnitude of the inertial oscillations. If surface waves contributed to the measured inertial currents, the processes just noted would cause a lowering of coherence between near inertial current shear and wind stress and the coherence would decrease substantially with depth. These comments do not hypothesize that wave caused inertial currents were important in the data analyzed by Rubenstein and Newman (1982) but are meant to indicate that wave caused inertial currents may account for some of the features. An analysis of meteorological conditions in the western North Atlantic Ocean and of hindcast wave data that are available would be needed to further investigate the importance of wave-caused inertial currents for this data set.

3. INTERNAL WAVES

A. INTRODUCTION

Internal waves may be generated by a variety of mechanisms which include: wind stress fields, atmospheric pressure fields, buoyancy fluxes, Ekman layer instabilities, bottom topographic effects, interactions with other internal waves, tidal flow over continental shelves, and interactions with surface gravity waves. There is considerable uncertainty about the relative importance of these mechanisms. The primary concern of this section is the upper ocean above a depth of a few hundred meters where atmospheric forcing generates internal waves. Although travelling wind stress and atmospheric pressure fields may directly generate internal waves in this region, the importance of these mechanisms depends on the spatial variation, temporal variation, and advection speed of these fields (e.g. Thorpe, 1975; Goodman and Levine, 1977). Because of the critical nature of this dependence and relatively small sea surface elevation changes caused by atmospheric pressure changes, travelling atmospheric pressure fields are probably less important than travelling wind stress fields. There is also evidence that travelling wind stress fields are better generators of higher-order internal wave modes than travelling atmospheric pressure fields (Goodman and Levine, 1977). Another mechanism, generation of internal waves by interaction with surface gravity waves, may be significant as a means to transfer atmospheric energy into internal waves. It is this mechanism which is discussed in this section. Of interest is the fact that surface gravity waves are almost always present and can have high wave heights during high wind speed events. Transfer of energy from surface gravity waves to internal waves may be a way to transfer atmospheric energy into internal waves without the limitations necessary for direct generation by wind stress or atmospheric pressure fields.

B. BASIC MECHANISMS

Two progressive surface gravity waves not travelling in the identical direction interact with an internal wave when the following conditions are met

$$\vec{k}_1 - \vec{k}_2 = \vec{k}_i \tag{3.1}$$

$$\sigma_1 - \sigma_2 = \sigma_i \tag{3.2}$$

where $\vec{k}_1$ and $\vec{k}_2$ are surface wave numbers, $\vec{k}_i$ is an internal wave number, σ_1 and σ_2 are surface wave radian frequencies, and σ_i is an internal wave radian frequency. In deep water, the dispersion relationship between surface wave frequency and wavenumber is given by

$$\sigma_1^2 = gk_1, \quad \sigma_2^2 = gk_2 \tag{3.3}$$

where g is acceleration due to gravity. The dispersion relationship between internal wave frequency and wave number depends on the density stratification. For a two-layer ocean in which the depth of a less dense surface layer is much less than the depth of a more dense deeper layer, the internal wave dispersion relationship is given by

$$\sigma_i^2 = gk_i^2 h(\Delta\rho/\rho) \tag{3.4}$$

where $\Delta\rho$ is the density difference between the layers, h is the upper layer thickness, and ρ is the density of the lower layer. It can be shown (e.g. Ball, 1964) that the frequency of

an internal wave that interacts with two surface waves is given by

$$\sigma_i = \sigma_1 - \sigma_2 = \frac{(\sigma_1+\sigma_2)^2 \sin(\theta/2)}{2\left\{\frac{g\rho}{h\Delta\rho}\right\}^{\frac{1}{2}}} \tag{3.5}$$

where θ is the angular difference between the propagation directions of the two surface waves.

Two surface waves with nearly the same frequencies can interact to transfer energy to a lower frequency internal wave. If the surface waves have a small angular separation, which often occurs in the ocean, Equation (3.1) shows that the interacting internal wave will travel at approximately right angles to the pair of interacting surface waves. This situation is shown schematically in Figure 3.1 where two surface waves are propagating in the directions of their vector wave numbers, $\vec{k}_1$ and $\vec{k}_2$, interact with an internal wave propagating in the direction of its vector wave number, $\vec{k}_i$. Surface wave directional spectra are generally spread about a primary direction which corresponds to the wind direction. Thus, surface waves with similar frequencies travel in somewhat different directions. These waves interact with internal waves travelling approximately perpendicular to the wind direction.

Equation (3.5) shows that one condition for surface wave frequencies is that

$$\sigma_1 \text{ and } \sigma_2 < \tfrac{1}{4}\left\{\frac{g\rho}{h\Delta\rho}\right\}^{\frac{1}{2}}\left\{1/\sin(\theta/2)\right\} \tag{3.6}$$

Surface wave spectra usually have a fairly sharp low frequency cut-off. Hence, except for wave components with very small angular separations, surface waves may not occur at

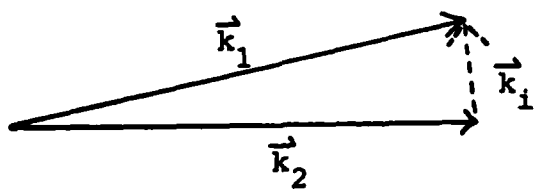

FIGURE 3.1. Interaction Diagram of Resonant Coupling Between Two Surface Waves With Wave Numbers, $\vec{k}_1$ and $\vec{k}_2$, and an Internal Wave With Wave Number, $\vec{k}_i$. The interacting internal wave propagates at nearly right angles to the interacting surface waves.

low enough frequencies to interact with internal waves. The importance of surface wave-internal wave interactions increases as the depth of the interface decreases. Since relatively high frequency surface waves are nearly always present, particularly in higher latitude storm track regions, surface wave-internal wave interaction may always occur for shallow interface depths representative of seasonal thermoclines. As low frequency surface wave energy increases, for example during higher wind speed events such as extratropical storms, there is increased capability for interaction between surface waves and internal waves at deeper depths.

The previous equations can be used to provide numerical examples of surface and internal wave interactions. For surface waves of approximately the same frequency ($\sigma_1 \simeq \sigma_2$) travelling at an angular separation, Θ, the interacting internal wave number magnitude from Equation (3.1) is given by

$$k_i \simeq \frac{2\sigma_1^2}{g} \sin(\Theta/2) \qquad (3.7)$$

and Equation (3.5) becomes

$$\sigma_i \simeq 2\sigma_1^2 \sin(\Theta/2) \left\{ \frac{h \Delta\rho}{g\rho} \right\}^{\frac{1}{2}} \qquad (3.8)$$

For h=20 m, $\Delta\rho/\rho$ =0.10, and surface waves with periods near 10 seconds (σ_1=0.628 radians-s^{-1}) travelling at an angular separation of 5°, the interacting internal wave has the following characteristics:

Internal wave number = k_i = 0.0035 m^{-1}

Internal wave length = $(2\pi)/k_i$ = 1,800 m

Internal wave frequency = $\sigma_i/(2\pi)$ = 0.0025 Hz = 8.9 c.p.h.

Internal wave period = $(2\pi)/\sigma_i$ = 404 s = 6.7 min. = 0.11 hours

For other selected values of surface wave frequencies, surface wave directions, and ocean stratification (e.g. h, ρ, and $\Delta\rho$ for this two-layer case), a wide range of interactions are possible. For typical wave directional spectra, there are wave components with suitable frequency and direction differences to interact with numerous internal waves with periods ranging from many seconds to on the order of an hour. In terms of internal waves, the internal waves that interact with surface waves are high frequency internal waves.

C. INTERNAL WAVE GENERATION

(1) TWO SURFACE WAVES

The previous description shows which waves interact but does not describe growth rates or amplitudes of the interacting internal waves. For this purpose, the simplest case is again that of two surface waves and a two-layer ocean. The internal wave amplitude initially grows at the following rate (e.g. Phillips, 1977)

$$\frac{\partial a_i}{\partial t} = \tfrac{1}{2}(1+\cos\Theta)\,(a_1 k_1)\,(a_2 k_2)\,(k_1 k_2)^{-\frac{1}{2}}\sigma_i \exp(-k_i h) \qquad (3.9)$$

where a is internal wave amplitude, t is time, Θ is the angle between two surface waves

with vector wave numbers $\vec{k}_1$ and $\vec{k}_2$, σ_i is the frequency of the internal wave, a_1 and a_2 are amplitudes of the surface waves, and h is the depth of the interface below the surface. A similar equation is given by Thorpe (1975). The requirements for surface wave-internal wave interactions noted in the last section must also hold. Equation (3.9) shows that the growth rate of internal waves depends on the slopes, a_1k_1 and a_2k_2, of the interacting surface waves. In terms of the surface waves, the internal wave growth rate is a second order effect which increases substantially from typically occurring low wave slopes on the order of 0.1 to maximum possible wave slopes approaching approximately 0.5. Wave slopes increase with sea state so that generation of internal waves by interaction with surface waves becomes more important for higher sea states than for lower sea states.

Equation (3.9) also demonstrates the importance of a shallow interface as was noted in the last section. The growth rate decays exponentially with the depth of the interface below the surface. For an interface depth more than one-half of an internal wave length, the decay factor is less than 0.043 (4.3%) indicating that internal wave generation by surface waves is not of much importance for deeper interface depths. The wave lengths of the internal waves are determined by equations in the last section. Representative surface wave conditions generally provide small growth rates for interface depths greater than 100 m.

Equation (3.9) is a complicated function of the angle, Θ, between the two surface waves since both k_i and σ_i, which can be written as a function of Θ, depend on Θ due to requirements for resonant interactions. As an example, for $\sigma_1 \simeq \sigma_2$, k_i is given by Equation (3.7) and σ_i has the same functional dependence on Θ as k_i due to the internal wave dispersion relationship, Equation (3.4). The surface wave direction difference, Θ, that provides the maximum growth rate is a function of the interface depth and the surface wave number but is typically much less than 90^o showing that internal waves are most

efficiently generated by surface waves with similar wave numbers but direction differences representative of actual surface wave directional spectra. Because water density differences are much smaller than the density difference between air and water, energy transferred from surface waves is usually negligible compared to the surface wave energy. Internal waves with substantial amplitudes may be generated with only a slight decrease in overall surface wave amplitudes. Energy is exchanged between interacting surface waves but this exchange is not of interest here.

For the previous numerical example, the initial growth rate is $a_1a_2(5.8\text{x}10^{-4})$ m-s^{-1} or $5.8\text{x}10^{-4}$ m-s^{-1} for a wave amplitude of 1 m. Multiplication of the growth rate by a time interval gives an estimate of the amplitude after the time interval. If there is surface wave energy at the interaction frequencies for time periods on the order of hours, resulting internal wave amplitudes can be on the order of meters. Higher wind speeds within extratropical storms generate such wave conditions. It seems that internal wave growth is not limited by the finite size of regions (i.e. near storms) in which higher than normal surface wave conditions occur. An appropriate time scale is the spatial scale of the high wave region divided by the group velocity at which internal wave energy is propagating through the region. For storm spatial scales of 10^5 to 10^6 m, this time interval is long. For a storm region on the order of 10^5 m in horizontal extent and a group velocity, $d\sigma_i/dk_i$, of 4 m-s^{-1} that corresponds to the previous numerical example, the time interval is $2.5\text{x}10^4$ s and the attained internal wave amplitude is roughly 15 m. This numerical example is a rough over-approximation because Equation (3.9) is the initial growth rate and no dissipation or dispersion of internal wave energy is considered. It is likely that internal waves generated during spatially and temporally short events, such as atmospheric frontal passages, may be limited by the time duration and/or spatial extent of the atmospheric disturbance.

As noted by Thorpe (1975), investigations for two surface waves interacting with an internal wave have been made by Thorpe (1966) and Nesterov (1972) for a two layer ocean and by Brekhovskikh et al. (1972) for a three layer ocean. Figure 3.2 shows the growth rate divided by $a_1 a_2 k_2 N$, where N is $(g(\Delta\rho/\rho)/h)^{1/2}$ for four cases. Case (a) is for a three layer ocean with the middle layer centered at a depth approximately corresponding to the wave length of the surface waves. Case (b) is for a two layer ocean with the interface at the same depth. Case (c) is for a three layer ocean with the middle layer centered at a depth approximately 2.5 times greater than the wave length of the surface waves. Case (d) is for a two layer ocean with the interface at the same depth. Comparison of curves (a) and (b) to curves (c) and (d) illustrate that resonant internal wave generation is most important for interfaces near the sea surface, i.e. relatively shallow seasonal thermoclines in the actual ocean. All of the curves show that the most efficient internal wave generation occurs for surface waves with relatively small direction differences. From the wave number requirement, Equation (3.1), for the resonant interaction, the resonant internal wave propagates at nearly right angles to the direction of the surface waves. For locally wind generated surface waves, the primary internal wave directions would be approximate right angles to the wind direction. Although differences between the two and three layer curves are not significant for qualitative comparisons, the differences illustrate that the actual density stratification should be more realistically considered for quantitative calculations needed for applications. For example, the growth rate at the peak for the shallow interface depth differs by approximately 50% for the two and three layer calculations.

Generation of an internal wave through interaction with two surface waves has been demonstrated in the laboratory by Joyce (1972, 1974). In this experiment with a very small wave tank (2 m in length, 1 m in depth, and 20 cm in width), the surface and internal waves were standing waves. With addition of a term $a_1 \delta$, accounting for viscous

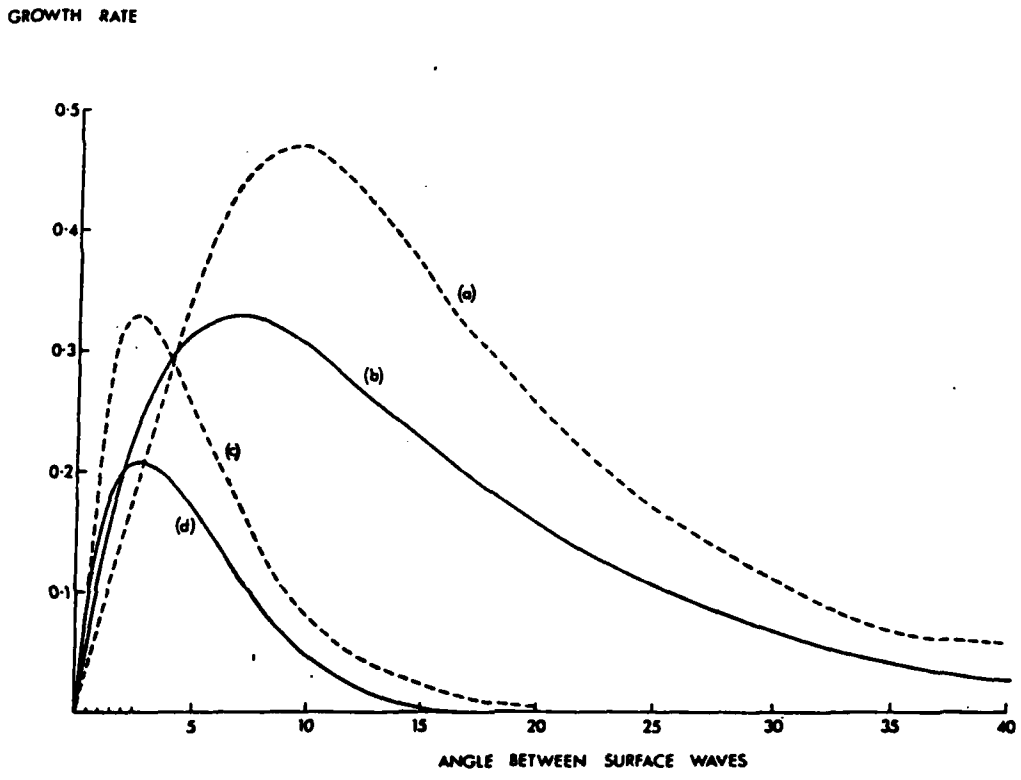

FIGURE 3.2. Growth Rates of Internal Waves Generated by Resonant Interactions With a Pair of Surface Waves for Various Density Stratifications as Described in the Text (from, Thorpe, 1975).

decay, the internal wave amplitude growth rate is given by

$$\frac{\partial a_i}{\partial t} + a_i \gamma = I a_1 a_2 \sigma_1 \sigma_2 \sigma_i \cos(\theta_1 - \theta_2 - \theta_i) \tag{3.10}$$

where a_i is internal wave amplitude, t is time, γ is a decay coefficient, I is an interaction term, a_1 and a_2 are the amplitudes of the surface waves, σ_1 and σ_2 are the radian frequencies of the surface waves, σ_i is the radian frequency of the internal wave, θ_1 and θ_2 are the phases of the surface waves, and θ_3 is the phase of the internal wave. The decay coefficient was determined by measuring the decrease of internal wave amplitudes after the wave generator that produced the interacting surface waves was turned off. For a two layer stratification and finite depth, the interaction term is given by

$$I = \frac{-\sinh k_i (H-h)}{2g \sinh(k_i H) \sinh(k_i h)} \tag{3.11}$$

where k_i is the wave number of the internal wave, H is the water depth (i.e. tank depth), and h is the interface depth. The similarity between Equation (3.9) which is for progressive waves, and Equations (3.10) and (3.11), which are for standing waves, can be seen by rewriting the last two equations for the deep water case as $k_i H$ becomes very large to yield

$$\frac{\partial a_i}{\partial t} + a_i \gamma = (a_1 k_1)(a_2 k_2)(k_1 k_2)^{-\frac{1}{2}} \sigma_i \cos(\theta_1 - \theta_2 - \theta_i) \exp(-k_i h) \tag{3.12}$$

While Joyce's results do not apply for progressive waves nor for deep water in

which the water depth is much greater than the wave lengths and the interface depth, reasonable agreement between his results and theory for the non-deep water standing wave situation implies that there might be similar agreement if the deep-water progressive wave situation could be simulated in the laboratory. Here, a few examples of Joyce's results as compared to theory are given. Figure 3.3 shows the steady-state internal wave amplitude response as the depth of the interface approaches the depth corresponding to the standing internal wave period that interacts with the surface waves. The theoretical curve for this interface depth is also shown. Figure 3.4 shows resonant growth of the internal wave as a function of time compared to the theoretical solution to Equation (3.10). Figures 3.5 and 3.6 show the amplitude response and growth rate when the surface wave frequencies and interface depth were selected to resonantly generate a second mode standing internal wave with a wave length one half as small as that of the first mode. Overall, Joyce's results provide evidence that internal wave generation through interaction with surface waves approximately agrees with theory for the simple standing wave two surface wave case that can be simulated in the laboratory.

Consideration of two surface waves shows that the following features apply to internal waves generated by surface waves:

-- Internal waves are high frequency internal waves with periods often on the order of minutes to an hour;

-- Most efficient generation occurs for a shallow interface representative of a seasonal thermocline;

-- Internal wave amplitudes may be on the order of meters;

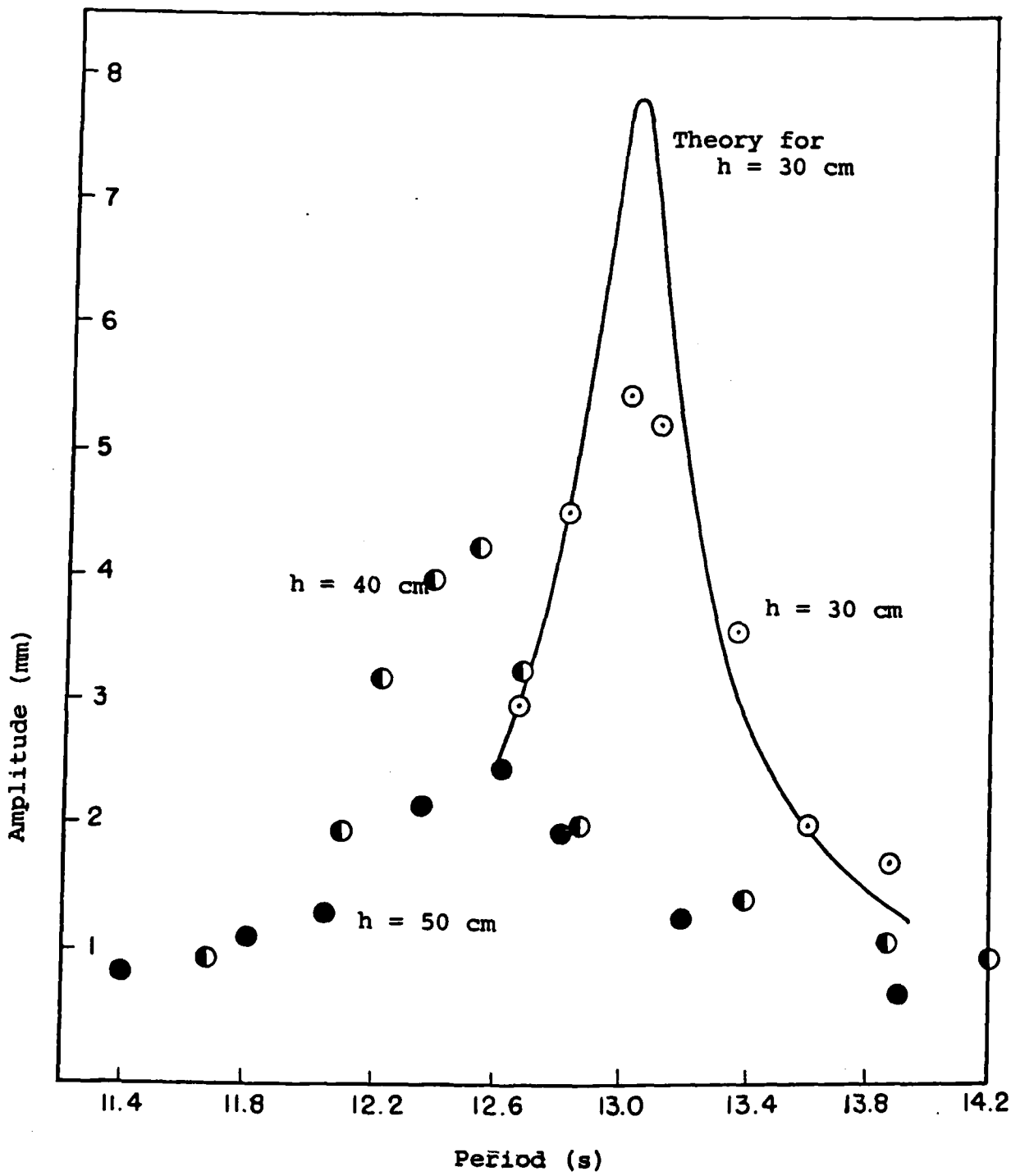

FIGURE 3.3. Internal Wave Amplitude Response as the Interface Depth in a Wave Tank is Raised Toward the Depth Corresponding to the Standing Internal Wave Period That Interacts With the Pair of Surface Waves (from Joyce, 1972, 1974). The response increases as the resonant depth is approached.

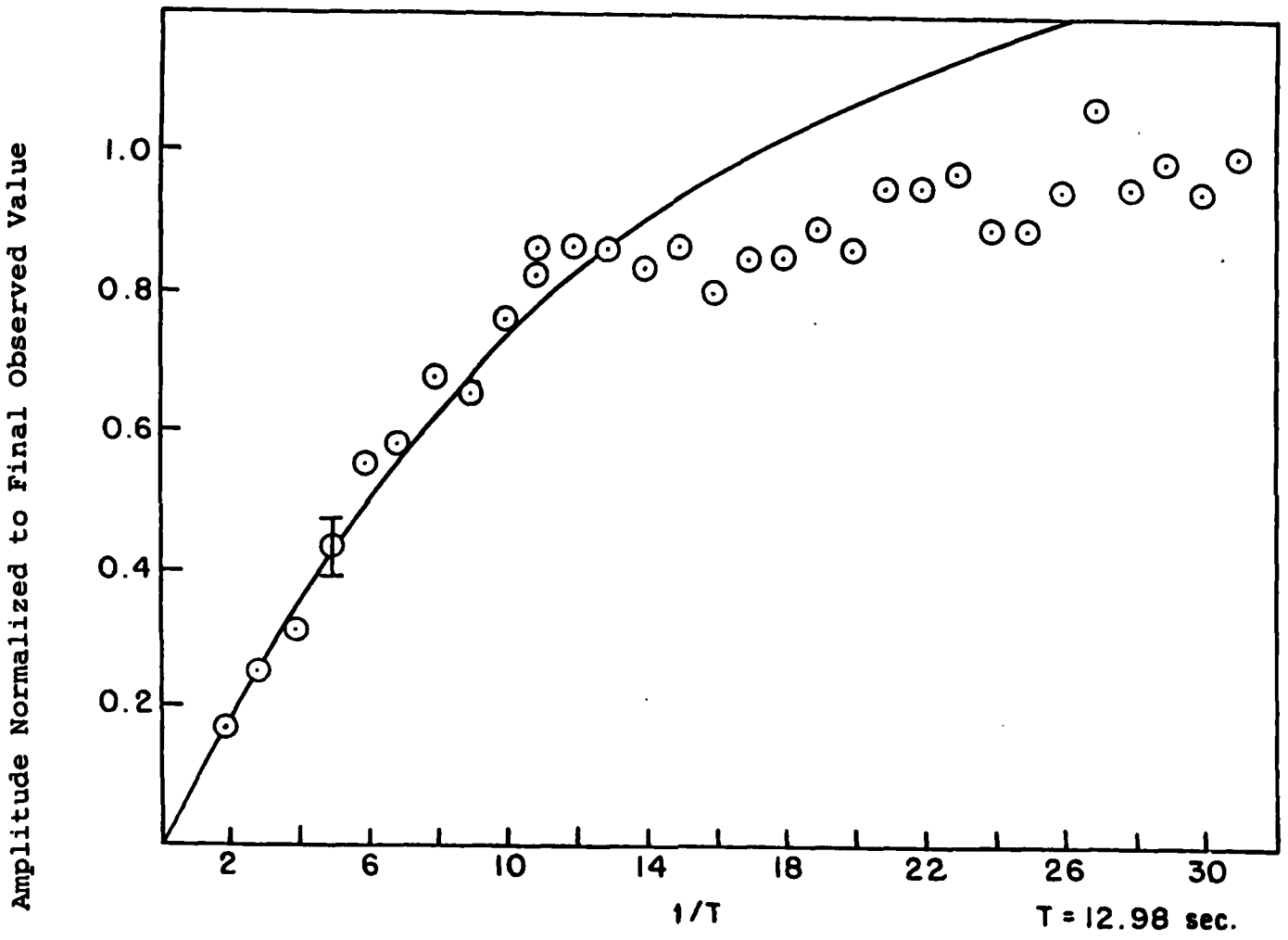

FIGURE 3.4. Resonant Internal Wave Growth in a Wave Tank as a Function of Time (from Joyce, 1972, 1974). The curve is the theoretical result.

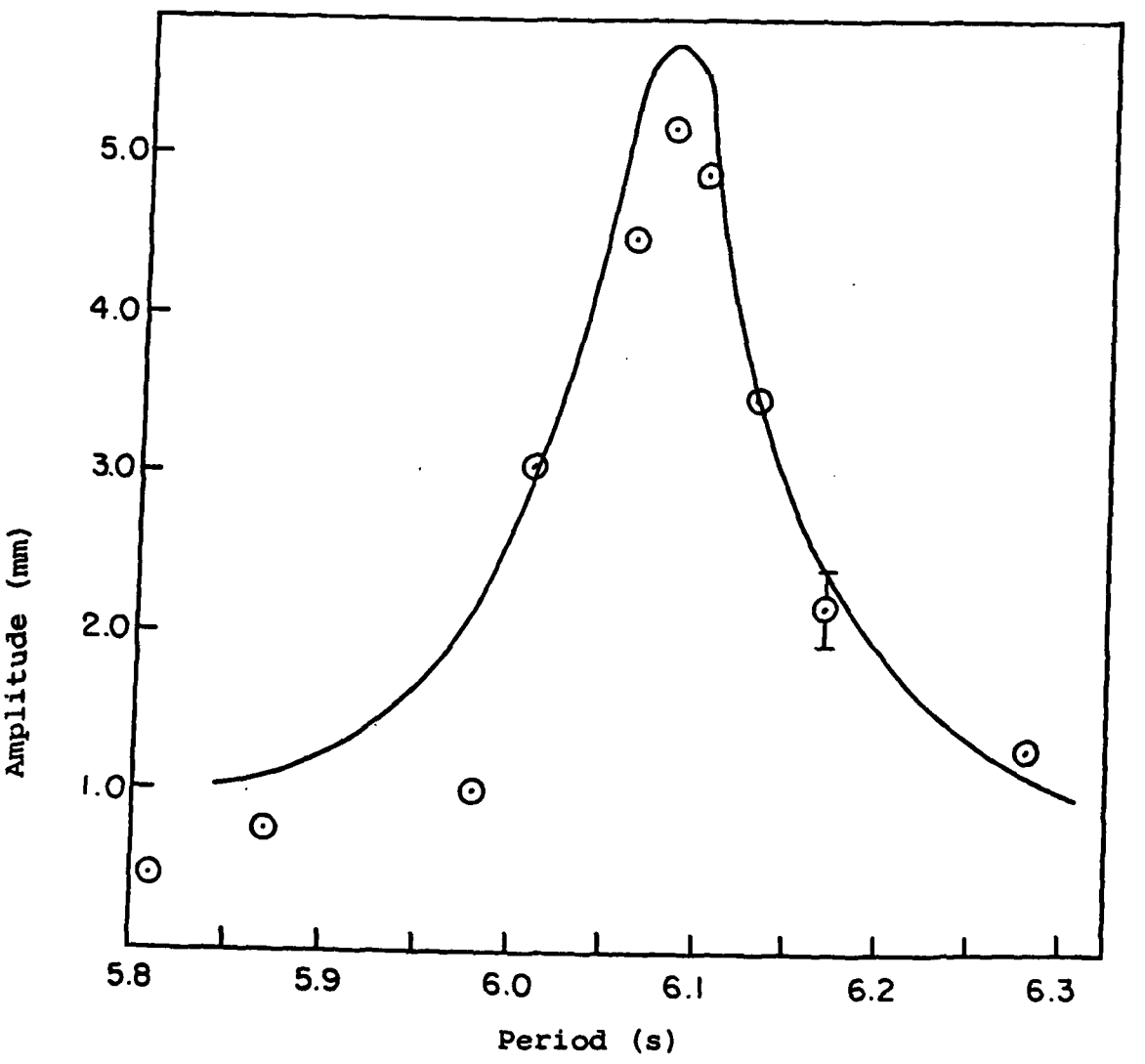

FIGURE 3.5. Internal Wave Amplitude Response for a Second Mode Standing Internal Wave Interacting With Two Surface Waves in a Wave Tank (from, Joyce, 1972). The curve is the theoretical result.

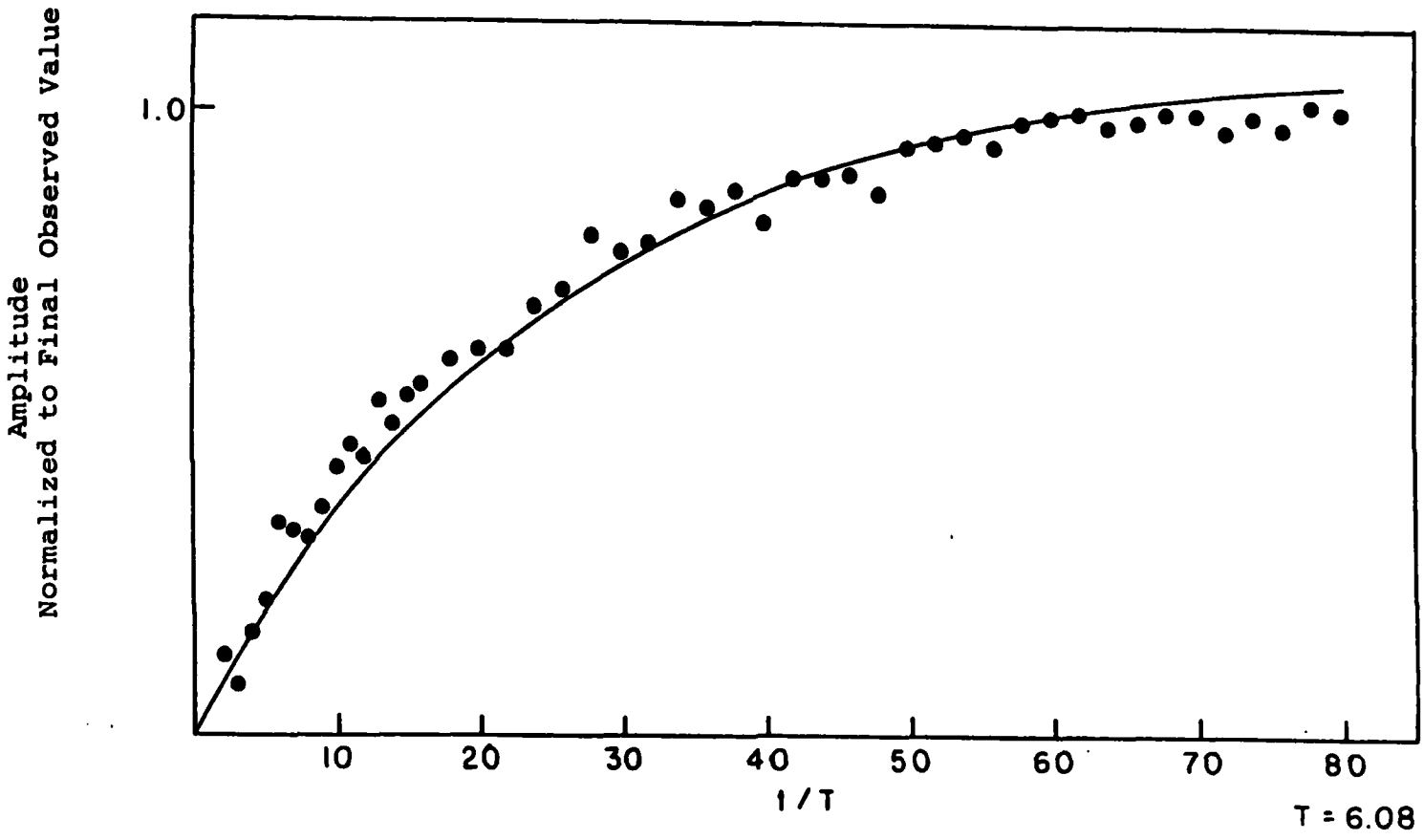

FIGURE 3.6. Resonant Second Mode Internal Wave Growth in a Wave Tank as a Function of Time (from Joyce, 1972, 1974). The curve is the theoretical result.

-- Propagation directions of internal waves are mainly perpendicular to the primary wave direction which is often near the wind direction; and

-- Internal wave generation is most important during high surface wave conditions such as within extratropical storms that occur in mid-latitudes and high latitudes.

(2) INTERACTION BETWEEN SURFACE AND INTERNAL WAVE SPECTRA

Both surface and internal waves are best described statistically by spectral concepts. The sea surface can be considered to consist of numerous wave components with different amplitudes, frequencies, directions, and phases (which are considered randomly distributed over 0 to 2π). As noted earlier, a wave directional spectrum provides the distribution of wave variance as a function of frequency and direction and can be written as a wave number spectrum. Analogous concepts hold for internal waves but other considerations, such as density stratification, become important. Internal waves can also propagate in both horizontal and vertical directions. It is impractical to calculate interactions between large numbers of surface and internal waves without making major simplifying assumptions so that a spectral approach is needed.

For analytical derivations, surface wave directional spectra due to locally generated seas are often used in the form

$$E(f,\Theta) = A(S(f)) \cos^{2S(f)}\left\{\frac{\Theta-\bar{\Theta}(f)}{2}\right\} \qquad (3.13)$$

where $E(f,\Theta)\, df d\Theta$ is the contribution to the wave variance from waves in the frequency interval, $f+df$, and the direction interval, $\Theta+d\Theta$, S is a spreading function and $\bar{\Theta}$ is the mean wave direction. In general both S and $\bar{\Theta}$ are functions of frequency so that A(S) is a function of frequency. Integration of $E(f,\Theta)$ over all directions (Θ to 2π) gives the wave frequency spectrum $E'(f)$ and it can be shown that

$$E(f,\Theta) = \frac{E'(f)}{2\pi^{\frac{1}{2}}} \frac{\Gamma(S(f)+1)}{\Gamma(S(f)+\frac{1}{2})} \cos^{2S(f)}\left\{\frac{\Theta-\bar{\Theta}(f)}{2}\right\} \qquad (3.14)$$

where Γ is the gamma function. Equation (3.13) is often simplified and written in the form

$$E(f,\Theta) = E''(f) \cos^{2S}\left\{\frac{\Theta-\bar{\Theta}}{2}\right\} \qquad (3.15)$$

where $\bar{\Theta}$ and S are independent of f, S and $\bar{\Theta}$ are empirically best-fit to data, and integration of $E(f,\Theta)$ over all directions gives the wave frequency spectrum. Equation (3.15) assumes that the distribution of wave energy by direction is the same at each frequency. This assumption is often not physically correct since high frequency locally-generated waves often have a broad directional spread (low S) while low frequency waves that have propagated from more distant generation regions often have a narrow directional spread (high S). Thus, surface wave directional spectra representations are available from which to estimate capability of surface waves to generate internal waves.

Hasselmann (1966) provided a general theoretical framework for describing spectral transfer rates due to most types of wave-wave interactions. This work has been applied to interactions of surface waves to show that interactions may be important in determining the surface wave frequency spectrum. This work has also provided much of the basis for development of the surface wave-internal wave interaction theories noted in this section.

Kenyon (1968) made an early calculation of energy exchange from a surface wave spectrum to an internal gravity wave spectrum. Internal wave spectra were obtained from measurements of vertical isotherm fluctuations from the U.S. Navy oceanographic tower in shallow water (depth = 18m) off Mission Beach, California. Surface wave frequency spectra were obtained from a wave recorder several miles away in shallow water

with a depth of 11 m. Surface waves were assumed to have an isotropic directional spectrum, which is unrealistic, and a directional spectrum of the form in Equation (3.15) with S=2. Internal wave growth rates were lower than subsequently calculated by others (e.g. Joyce, 1974; Watson et al., 1976; Olbers and Herterich, 1979) because Kenyon used an assumption of constant Brunt-Vaisala frequency over depth. As noted by Joyce (1974), the interaction coefficient is far greater for a two-layer ocean with a shallow thermocline than for an ocean with a constant Brunt-Vaisala frequency. Presence of a shallow thermocline causes an overlap of the region of surface wave forcing and internal wave motion which is largest near the thermocline. While Kenyon's calculations of surface and internal wave interactions did not account for the level of the internal wave spectra, they illustrated several surface wave-internal wave interaction features. Most importantly, interactions between surface waves with similar frequencies and directions generate internal waves propagating perpendicular to the primary wave direction, and the energy transfer rate to the first internal wave mode is much greater than to the second internal wave mode. In addition, calculations showed that the time scale of energy transfer from surface to internal waves is much longer than the redistribution of energy among internal waves due to internal wave interactions although for the deep ocean this conclusion is affected by the lower internal wave growth rates due to the constant Brunt-Vaisala frequency assumption.

A more detailed calculation of interactions between surface and internal gravity waves was made by Watson et al. (1976). In their numerical calculations, density stratification was represented by two cases: a zero Brunt-Vaisala frequency above a thermocline with an exponentially varying Brunt-Vaisala frequency below the thermocline, and a two layer model with a non-zero Brunt-Vaisala frequency only at the thermocline. Figure 3.7 shows a time scale, called the growth time, which is the internal wave energy divided by the rate of energy input as a function of wave number for the three lowest

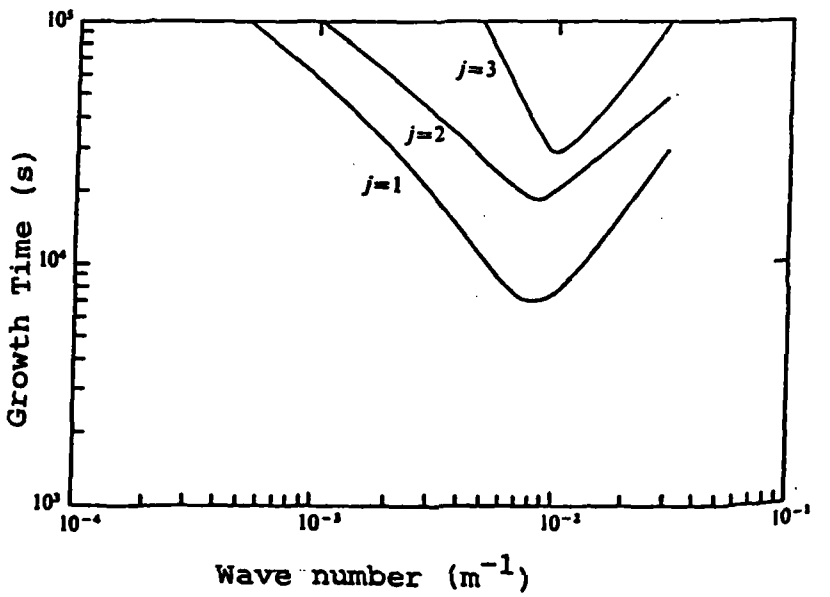

FIGURE 3.7. Growth Time of the Three Lowest Internal Wave Modes (j=1,2,3) as a Function of Wave Number (from Watson et al., 1976). The lowest mode grows fastest.

internal wave modes. An equilibrium surface wave spectrum, such as that later noted in Section 4-B, and the first density stratification case were used. The growth times are shortest for the lowest mode. These growth times which are on the order of a few hours to a day are considerably shorter than growth times that would result from subsequent work by Olbers and Herterich (1979) for the type of high frequency equilibrium wave spectrum used by Watson et al. as the surface wave spectrum. As noted by Olbers and Herterich, the discrepancy is likely caused by the use of a finite number of specified surface wave components with particular frequencies, directions, and phases in the work of Watson et al. In the actual ocean, wave phases are random and individual wave components do not retain constant phase relationships for time periods long compared to surface wave-internal wave interaction times. Nevertheless, the work of Watson et al. demonstrates the importance of a relatively shallow thermocline, a highest growth rate for the lowest internal wave mode, and generation of internal waves propagating perpendicular to the primary surface wave direction. Although the work is useful as an indicator of general features of surface and internal wave interactions and the work could be up-dated, deterministic calculations of the interactions and use of simplied forms of the surface wave directional spectrum prevent using the work for quantitative evaluation of internal wave generation by realistic sea states.

Olbers and Herterich (1979) derived equations for the initial growth of the wave number spectrum of internal waves due to interaction with a surface wave number spectrum. The general result is a complicated function of the surface wave number spectrum and the density stratification and must be evaluated numerically. However, since the internal wave frequencies and wave numbers are substantially lower than the frequencies and wave numbers of surface waves, simplifications can be made. The initial growth rate of the internal wave spectrum for vertical mode, λ, is given by

$$s^{\lambda}(k,\phi) = 16\pi E''^{2}(k_m/g)^{\frac{1}{2}} \int_0^{\infty} x^{3/2} G^2(x) H^{\lambda}(x,k) \sum_{s=+-} A^2(\phi + \tfrac{1}{2} s\pi, xk_m)\, dx \qquad (3.16)$$

where the surface directional spectrum is written as

$$E(k,\Theta) = E'(k) A(\Theta,k) \qquad (3.17)$$

with

$$E'(k) = (E''/k_m) G(k/k_m) \qquad (3.18)$$

and ϕ is internal wave direction. K_m is the surface wave number corresponding to the spectral maximum where G is normalized to unity. This normalization facilitates understanding of the spectral results based on simple analytical spectral formulations that have been empirically derived for surface waves but may not be particularly useful in working with measured or hindcast directional spectra. The directional spectra used by Olbers and Herterich can be placed in the form of Equation (3.13) with scalar wave number and direction used in place of frequency and direction. The function, $H^{\lambda}(x,k)$ is a function of Brunt-Vaisala frequency, vertical structure of the internal wave mode λ, the top depth of a thermocline region where the Brunt-Vaisala frequency is non-zero, the

bottom depth of this region, and k_m.

A few illustrative results from Olbers and Herterich are given here. Figures 3.8 and 3.9 show surface wave frequency spectra and directional spreading functions used by them. Figure 3.10 is a plot of the initial growth rate for the lowest internal wave mode for a Brunt-Vaisala frequency of 15 c.p.h. between 50 m and 100 m depth and zero elsewhere. The ocean depth is 5,000 m, the utilized surface wave spectrum is labelled PL in Figure 3.8, and the utilized spreading function is labelled A_2 in Figure 3.9. As inferred from simpler theory, the maximum growth rate occurs approximately perpendicular, $\pi/2$ in Figure 3.10, to the primary direction of the surface waves. Figure 3.11 is the wave number spectrum, i.e. $S(k,\Phi)$ integrated over Φ, corresponding to Figure 3.10. The wave length of internal waves corresponding to the maximum growth rate is about 600 m. Results based on the other surface wave frequency spectra in Figure 3.8 differed by less than 10% and results based on the other spreading functions in Figure 3.9 differed by less than 1%. The relatively low sensitivities to the frequency and directional variations of the surface wave spectra is due to the importance of interactions between surface waves with similar directions and between surface waves with similar frequencies to generate internal waves with appropriate frequencies and wave numbers for the given density stratification. However, while Olbers and Herterich conclude that only bandwidths rather than shapes of the frequency spectra and spreading functions are important, this conclusion may not be valid for actual surface wave spectra which often do not have smooth single-peaked forms.

Figure 3.12 shows the internal wave frequency spectrum growth rate for the lowest three modes to illustrate faster growth of the lowest mode. Kenyon (1968) and Watson et al. (1976) also showed more rapid growth for lower modes than for higher modes. Figure 3.12 indicates an approximate order of magnitude difference between growth rates

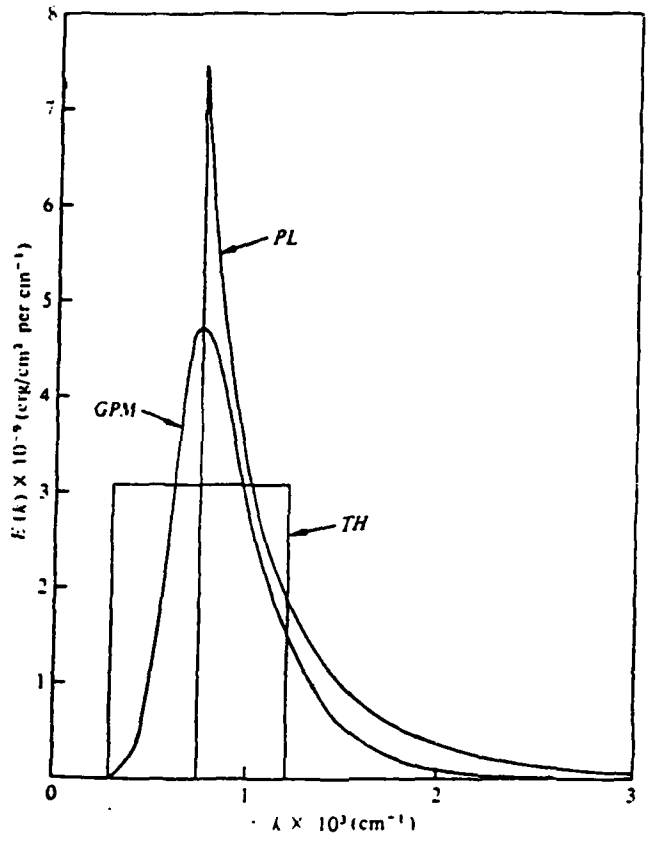

FIGURE 3.8 Wave Number Spectra Used by Olbers and Herterich (1979). The spectra have similar relative appearances when converted to frequency spectra.

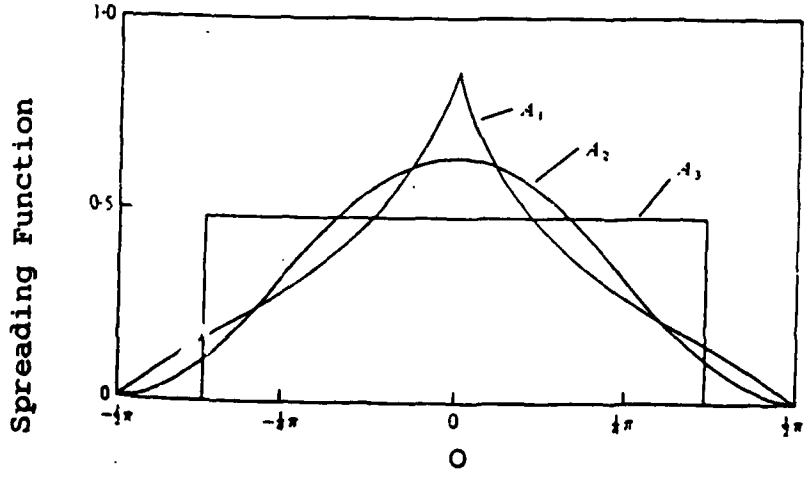

FIGURE 3.9. Directional Spreading Functions Used by Olbers and Herterich (1979).

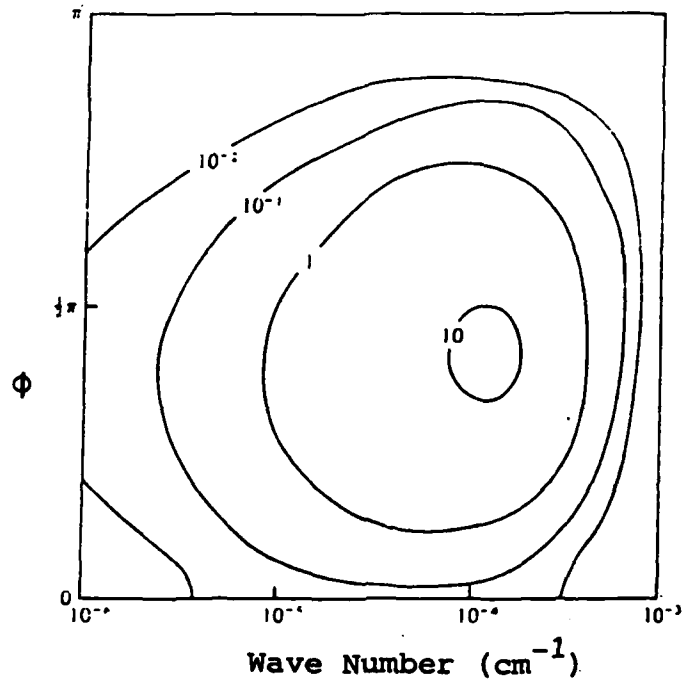

FIGURE 3.10. Example of Initial Growth Rate of Lowest Internal Wave Mode (from, Olbers and Herterich, 1979). The maximum growth rate is perpendicular to the primary wave direction.

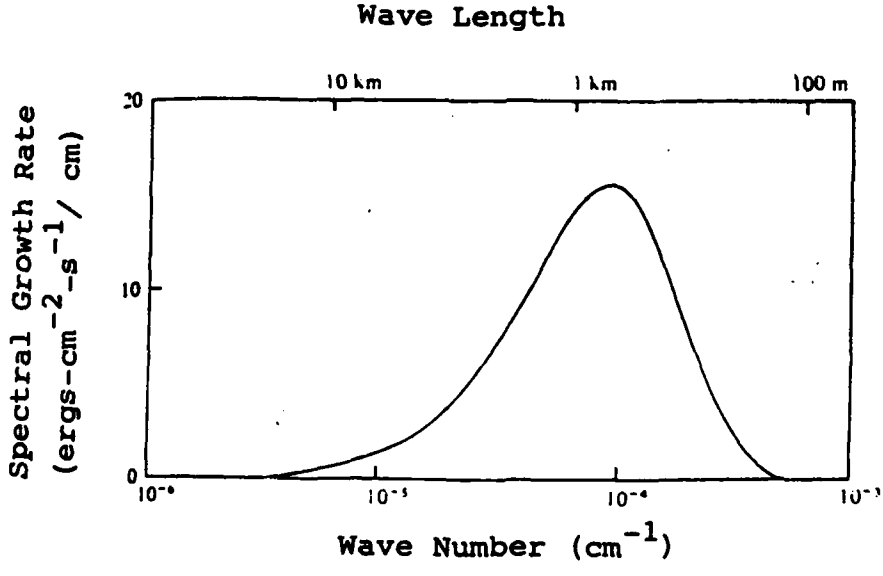

FIGURE 3.11. Corresponding Wave Number Growth Rate Integrated Over Direction (from Olbers and Herterich, 1979). The wave length with the maximum growth rate is about 600 m.

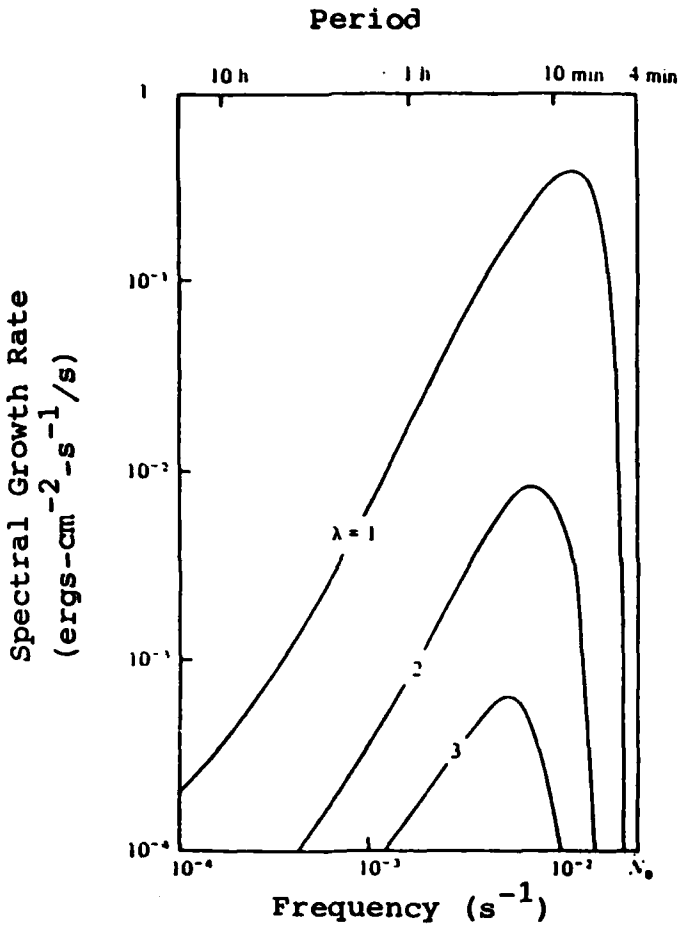

FIGURE 3.12. Internal Wave Frequency Spectrum Growth Rate for the Three Lowest Modes (from Olbers and Herterich, 1979). The lowest mode (λ=1) has the fastest growth rate.

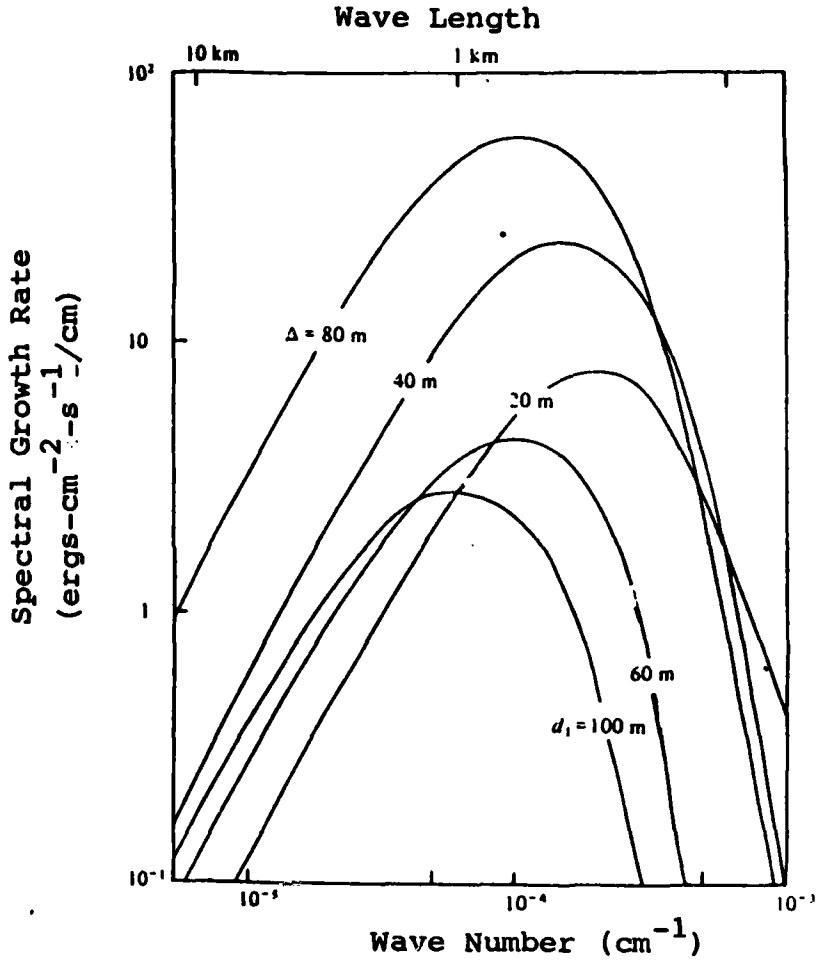

FIGURE 3.13. Effects of Thermocline Thickness (Δ) and Depth (d_1) on the Initial Growth Rate of the Lowest Mode (from Olbers and Herterich, 1979). The top three curves have d_1=60 m and the lower three curves have Δ=20 m.

for different modes. A representative frequency of most rapid growth is between 4 to 6 c.p.h. Thus, the generated internal waves are high frequency internal waves.

Effects of seasonal thermocline thickness and depth on the initial growth rate for the lowest mode are shown in Figure 3.13. For the upper three curves, the depth of the top of the thermocline, which is considered as the region with constant Brunt-Vaisala frequency, is 20 m. The growth rate increases as the thickness increases. For the lower three curves (the middle curve is in each set of three) the thickness is 20 m. The growth rate increases as the depth decreases which is consistent with results for a pair of surface waves. If the thermocline depth is further increased to represent the main thermocline, the growth rate continues to decrease so that internal wave generation through surface wave interactions is not important.

A useful calculation made by Olbers and Herterich is the total transfer rate, due to all frequencies or wave numbers, for the lowest modes as a function of several types of density stratification. These results are given in Table 3.1 for the two lowest modes. Transfer rates for the next mode are even lower than for these modes. Input wave spectra had a cosine-squared directional spreading function, i.e. S=1 in Equation (3.13), and a JONSWAP (Joint North Sea Wave Project) frequency spectrum. The JONSWAP spectrum, which was developed for fetch-limited waves, is not necessarily typical of wave spectra in storm track regions of the North Atlantic and North Pacific Oceans. Root-mean-square wave height for the input spectra was 1.1 m and significant wave height was 1.6 m. While such heights often occur, these wave heights are not representative of fairly frequently occurring higher wave heights. Table 3.1 demonstrates several important features. For a constant Brunt-Vaisala frequency ocean, growth rates are much lower than for a more realistic ocean with a thermocline. Growth rates for a main, or deep, thermocline are orders of magnitudes lower than growth rates for a seasonal, or shallow,

TABLE 3.1.

Energy Transfer Rates to the Two Lowest Internal Wave Modes for Several Types of Density Stratification (after Olbers and Herterich, 1979).

Stratification Type	Brunt-Vaisala Frequency (c.p.h.)	Depth to Top of Thermocline (m)	Thermocline Thickness (m)	Energy Transfer Rate (ergs-cm^{-2}-s^{-1})	
				$\lambda=1$	$\lambda=2$
Constant	1	0	5000	$3.1\cdot10^{-6}$	$1.5\cdot10^{-6}$
Main Thermocline	3	100	900	$3.2\cdot10^{-4}$	$8.4\cdot10^{-5}$
" "	3	500	500	$7.3\cdot10^{-5}$	$1.2\cdot10^{-6}$
Seasonal Thermocline	15	25	50	$5.7\cdot10^{-2}$	$1.4\cdot10^{-3}$
"	15	50	50	$3.7\cdot10^{-2}$	$4.2\cdot10^{-4}$
"	20	25	50	$1.8\cdot10^{-1}$	$4.3\cdot10^{-3}$
"	20	50	50	$1.2\cdot10^{-1}$	$1.3\cdot10^{-3}$

thermocline. As inferred from the two surface wave case, growth rates for a seasonal thermocline depend on details of the stratification (i.e. Brunt-Vaisala frequency and thermocline depth in Table 3.1).

A rough estimate of internal wave amplitudes can be made from the growth rates in Table 3.1. Use of the same time interval, 2.5×10^4 s, from Section C-(1) with growth rates of 10^{-1} and 10^{-2} ergs-cm^{-2}-s^{-1} yields energy values of 2.5×10^3 and 2.5×10^2 ergs-cm^{-2}. For the 15 c.p.h. Brunt-Vaisala frequency, the density difference across the thermocline is about 9×10^{-5} gm-cm^{-3}. Internal wave energy is given by $g(\Delta\rho)Z^2$ where $\Delta\rho$ is the density difference and Z^2 is a time average of the internal wave elevation squared. A root-mean-square elevation is given by Z. The resulting elevations for the two energy levels are approximately 55 cm and 170 cm showing that internal wave elevations may be on the order of meters as found for the two surface wave case.

Equation (3.16) shows that higher growth rates occur for higher wave heights than were used to develop Table 3.1 . From this equation and the dispersion relationship for surface waves, the internal wave energy growth rate is proportional to $E_S^2\sigma$ where σ is the surface wave frequency near the spectral peak and E_S is total surface wave energy. Since E_S is proportional to wave variance, the internal wave energy growth rate is proportional to the fourth power of surface wave height. The internal wave amplitude growth rate is proportional to the second power of surface wave height as earlier shown for two surface waves. Thus, internal wave generation through interaction with surface waves becomes a much more important process during higher wave conditions than during lower wave conditions. Olbers and Herterich note that the internal wave energy growth rate for Pierson-Moskowitz and JONSWAP surface wave spectra is proportional to the seventh power of the wind speed. This occurs because E_S is proportional to the fourth power of wind speed and σ is proportional to the reciprocal of wind speed. Hence, the

generation process is more important by orders of magnitude during high wind speed events than during typical low wind speed events. For example, doubling the wind speed increases the energy growth rate by roughly a factor of one hundred.

As earlier noted, energy lost by surface waves to internal waves is negligible in comparison to the surface wave energy but can result in appreciable internal wave amplitudes due to the relatively small density difference across a two layer interface compared to the density difference between water and air at the sea surface. The work of Olbers and Herterich show the same results with the growth rate of the internal waves being negligible compared to the energy of the surface waves but non-negligible compared to the internal wave energy. If a time scale is defined as the ratio of the total energy divided by the growth rate, the time scale for extraction of energy from surface waves is on the order of months while the time scale for addition of energy to internal waves can be fractions of days for higher surface wave conditions. The shortness of the internal wave time scale shows that substantial internal wave generation can occur during episodes of higher wave conditions such as during storms.

D. VERIFICATION BY MEASUREMENTS

Generation of internal waves through interaction with surface waves has not been verified by oceanic measurements. A practical problem is the difficulty, particularly with moored sensors, of making reliable internal wave measurements in the upper 100 m where surface wave orbital motion and higher speed wind-driven currents may cause mooring motion. A scientific problem is that other generation mechanisms, primarily internal wave generation by surface wind stress, may occur at the same time as surface waves that generate internal waves. For example, the previous descriptions show that internal wave generation through interaction with surface waves should be important near storm regions

with high wave heights. Yet, these same storms are travelling regions of higher than normal wind stress. In addition, interactions among internal waves tend to rapidly destroy characteristics of internal waves that are tied to the generation mechanism by distributing wave energy among internal wave components. Although time varying energy is transferred from surface to internal waves, ultimate internal wave characteristics are more determined by slowly varying internal oceanic features such as density stratification. Roth et al. (1981) provide some discussion of these points in their hypothesis that internal waves in the upper ocean can be represented as spectral fluctuations superimposed on a base state stationary spectrum such as variations of the Garrett and Munk model. Roth et al. show several examples of upper ocean spectra with higher energies than the Garrett and Munk model. Of considerable interest is the fact that the positive deviations of the upper ocean spectra from the Garrett and Munk model are often largest at higher frequencies where internal waves may be generated through interaction with surface waves. Figures 3.14 and 3.15 are two such examples.

Kase and Clarke (1978) discuss high frequency internal waves (frequencies greater than approximately 2 c.p.h.) in the seasonal thermocline during the GATE experiment. Data consisted of temperatures from moored sensors and CTD profiles. A primary spectral peak was found between 2 and 5 c.p.h. and a secondary spectral peak was found near 12 c.p.h. The high frequency internal waves are low mode, have amplitudes of 1 to 2 m, and are non-stationary over time periods of a day and less. While Kase and Clarke do not emphasize the generation mechanism, the energy spectra are shown to be consistent with wind stress forcing and the Brunt-Vaisala profile at the location. However, the energy spectra, particularly the 12 c.p.h. peak, may also be accounted for by generation through surface wave interactions. Whether this is true or not, the data set indicates seasonal thermocline internal waves at frequencies that would be generated by surface wave interactions.

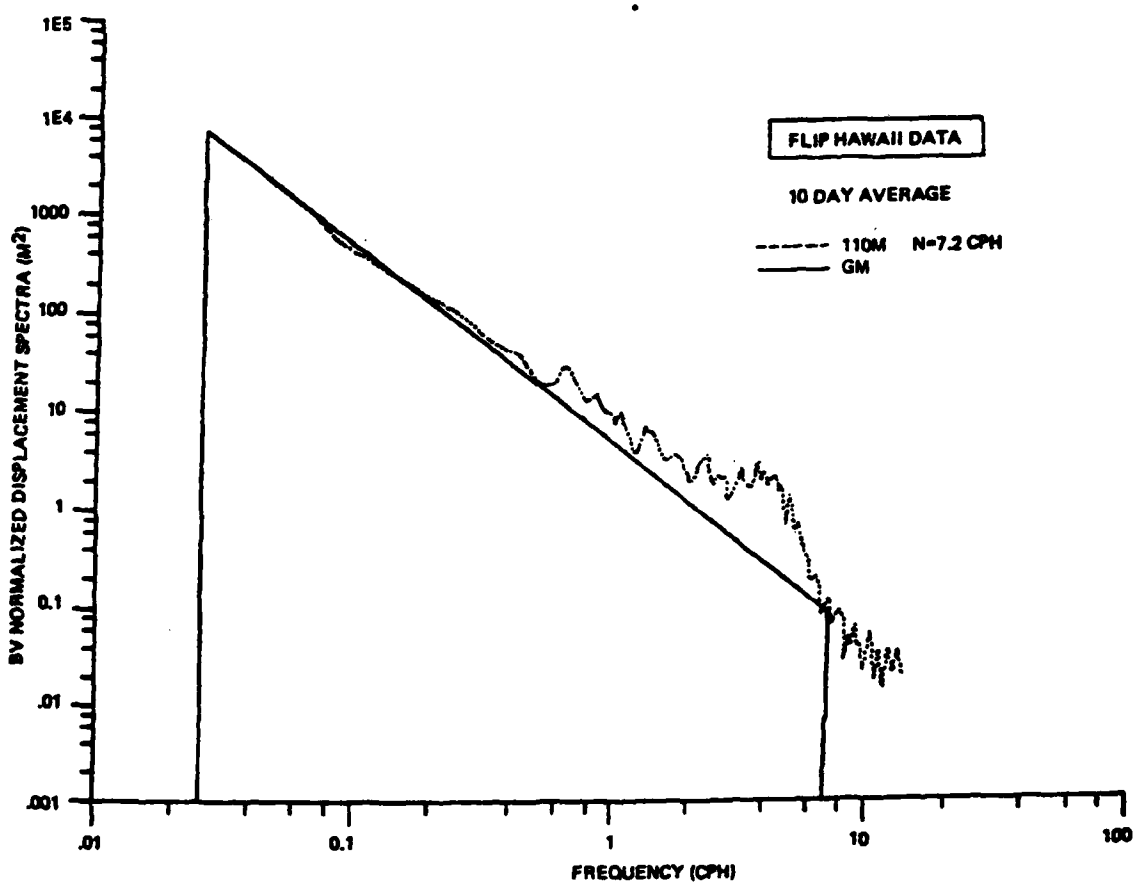

FIGURE 3.14. Example of Internal Wave Spectrum With High Frequency Energy Above the Garrett and Munk (GM) Model (from Roth et al., 1981).

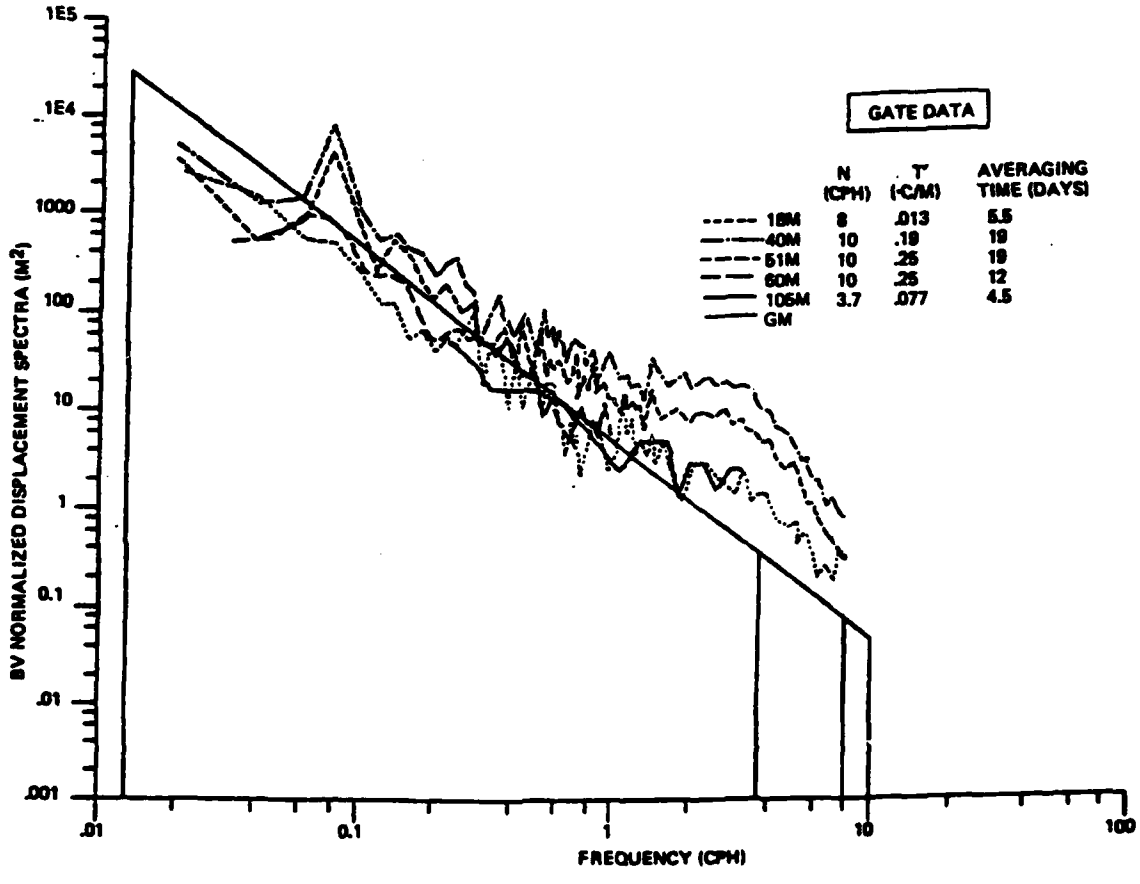

FIGURE 3.15. Other Examples of Internal Wave Spectra With High Frequency Energy Above the Garrett and Munk (GM) Model (from Roth et al., 1981).

Measurements during two storm events that occurred in the Mixed Layer Experiment (MILE) are described by Davis et al. (1981a). Although temperature and velocity spectra show a decrease above 3 cph, high frequency contributions consistent with low mode internal waves in the seasonal thermocline were observed. Velocity spectra (not internal wave amplitude spectra) between 7 cph and 30 cph were roughly proportional to wind speed squared and increased by a factor of about 20 between the most major storm event and quieter periods between storms. While Davis et al. note that this energy seems wave-related, no attempt was made to compare features of the high frequency motion with characteristics of internal waves produced through interactions with surface waves. Additional analysis results than those presented by Davis et al. are needed to make such comparisons. The location of the measurements near Ocean Station P in the North Pacific ocean is representative of locations of interest to the OMP.

Other results from the MILE experiment were previously described by Dillon and Caldwell (1980) and are also consistent with possible generation of internal waves by means of interactions with surface waves. Measurements of temperature, pressure, and drop speed from a free falling probe showed dominance of first and second internal wave modes at relatively high frequencies of 2.5 cph to 4 cph. These measurements were made during relatively low wind speed and wave height conditions between the storms described by Davis et al. (1981a) so that surface wave effects would have been greatly reduced compared to effects during the storms.

Apel et al. (1975) show an example of an image from the earth Resources Technology Satellite (ERTS-1) that has surface and internal wave patterns consistent with internal wave generation by resonant interaction with surface waves. The patterns may be accounted for by internal waves propagating at nearly right angles to the mean surface wave direction.

No internal wave data set seems to have been analyzed specifically with the goal of determination of the importance of surface waves in generating internal waves. Such an analysis was beyond the scope of this project. Selection of candidate data sets is the first step. Candidate data sets must be near surface measurements (i.e., within and above the seasonal thermocline) and should be accompanied by wind and wave measurements. Weather charts should be used with the candidate data sets to select data sets for which wind stress and surface wave-internal wave interaction generation mechanisms are likely present in different degrees of relative importance. For example within a storm region, both wind stress and surface wave effects may be important while close to, but not within the region, wave effects may be more important than wind stress. If propagation directions of internal waves are measured, cross-spectral or correlation analyses analysis of wind and internal wave directions would be useful since internal waves generated through interaction with locally-generated surface waves would be propagating roughly perpendicular to the local wind direction. The local wind direction could be measured or calculated from weather charts. Cross-spectral analysis between fluctuations in high frequency internal wave energy and wind stress (or wind speed) may provide different results than cross-spectral analysis between the internal wave energy and surface wave energy (or appropriate powers of surface wave energy). Higher coherences between the energy of surface and internal waves than between wind stress and internal wave energy could indicate that the interaction generation mechanism does not have limitations as stringent as the direct wind stress generation mechanism.

4. WAVE EFFECTS ON VERTICAL DISTRIBUTIONS

A. INTRODUCTION

Previous sections describe the role of surface waves in generation of inertial currents and internal waves. These sections represent the primary emphasis of this project. A secondary part of this project was a review of surface wave effects on mixing and turbulence which modify the distribution of not only current shear but also other parameters such as temperature and salinity. This is an area in which scientific knowledge is poor and in which there are inadequate theoretical relationships from which to make quantitative calculations for applications. One major problem is difficulty in making turbulence measurements near the sea surface in the presence of waves, especially in deep water where there are not fixed platforms on which to attach sensors. This problem is compounded by the fact that the processes of interest are generally second order effects in terms of wave theory and become significanty more important for higher wave heights when upper ocean measurements are most difficult. Because wave heights, and wave effects on mixing and turbulence, increase with wind speed, theoretical and numerical upper ocean models may avoid consideration of wave effects yet implicitly include such effects through model wind speed dependence.

B. WAVE BREAKING

Wave breaking is an obvious source of turbulence near the sea surface. As pointed out by Phillips (1977) on the basis of order of magnitude estimates, the energy flux from the wind to the waves may be comparable or greater than the direct energy flux from the wind to ocean currents. Energy, in the form of small-scale turbulence, is injected into the near surface region as waves break sporadically in both space and time. For growing

wave conditions, there may be a time period when a considerable portion of the energy flux from the wind goes into waves rather than into currents. For steady-state conditions, nearly all of the energy flux from the wind may go into currents partly through the intermediate process of wave breaking. Although wave breaking is most noticable during storm conditions, less visually obvious wave breaking occurs during low wind speeds for high frequency waves which exceed breaking criteria when the wave spectrum is fully-developed.

A progressive wave breaks when the downward acceleration at a crest exceeds one-half of the acceleration due to gravity. Longuet-Higgins (1969) used this criterion and a Rayleigh distribution of wave amplitudes to show that the mean loss of wave energy per wave cycle due to breaking is given by

$$\bar{E} = E \exp(-E_o/E) = \bar{\omega} E \tag{4.1}$$

where

$$E = \rho g \int_0^\infty E(\sigma)\, d\sigma = \text{total wave energy} \tag{4.2}$$

$$E_o = \frac{1}{8} \rho g^3 \bar{\sigma}^{-4} \tag{4.3}$$

and

$$\bar{\omega} = \text{fraction of wave energy lost per wave cycle} \tag{4.4}$$

The water density is given by ρ, g is the acceleration due to gravity, E is the wave frequency (radians) spectrum, and $\bar{\sigma}$ is a zero-crossing frequency given by

$$\bar{\sigma}^2 = \frac{\int_0^\infty \sigma^2 E(\sigma)\, d\sigma}{\int_0^\infty E(\sigma)\, d\sigma} \tag{4.5}$$

An equilibrium spectrum with a sharp low frequency cut-off at $\sigma=\sigma_1$, is given by

$$E(\sigma) = \alpha g^2 \sigma^{-5} \quad \text{for } \sigma \geq \sigma_1 \tag{4.6}$$

$$E(\sigma) = 0 \quad \text{for } \sigma < \sigma_1 \tag{4.7}$$

where α is an approximate constant that is sometimes called the Phillips or equilibrium range constant. The functional form of Equation (4.6) results because waves are limited by breaking. Therefore, the spectrum is said to be saturated. For this spectrum,

$$\bar{\omega} = \exp(-1/8\alpha) \tag{4.8}$$

which is independent of the cut-off frequency. Use of a representative value of $\alpha = 1.23\ 10^{-2}$ (Phillips, 1977) yields $\bar{\omega} = 3.9\ 10^{-5}$.

A Pierson-Moskowitz (1964) spectrum for fully-developed waves is given by

$$E(\sigma) = \frac{\alpha g^2}{\sigma^5} \exp\left\{-\beta(\sigma_o/\sigma)^4\right\} \tag{4.9}$$

where $\alpha = 8.10\ 10^{-3}$, $\beta = 0.74$, $\sigma_o = g/u$, and u is wind speed at an elevation of 19.5 m above the sea surface. For this spectrum

$$\bar{\omega} = \exp(-1/(2\pi\alpha)) = 2.9 \cdot 10^{-9} \tag{4.10}$$

which is independent of β and σ_o. The fraction of energy lost per wave cycle from a Pierson-Moskowitz spectrum is less than from an equilibrium spectrum because a Pierson-Moskowitz spectrum contains additional energy at lower frequencies (longer wave lengths) where waves are not breaking.

The rate of energy loss, E, per time is $\bar{\omega}E$ divided by the wave period associated with $\bar{\sigma}$. For an equilibrium spectrum, $\bar{\sigma} = (2)^{1/4}\sigma_1$, and σ_1 is approximately given by g/u. The rate of energy loss is

$$\dot{E}_{equilibrium} = \frac{\bar{\omega}\alpha\rho u^3}{2^{5/2}\pi} = 2.74 \cdot 10^{-8} u^3 \tag{4.11}$$

The analogous result for a Pierson-Moskowitz spectrum is

$$\dot{E}_{PM} = \frac{\bar{\omega}\,\alpha\rho u^3}{8(\pi\beta)^{3/4}} = 1.60 \cdot 10^{-12} u^3 \qquad (4.12)$$

As a numerical example, for a wind speed of 1000 cm-s^{-1} (approximately 20 knots)

$$\dot{E}_{equilibrium} = 27 \text{ ergs-cm}^{-2}\text{-s}^{-1} \qquad (4.13)$$

$$\dot{E}_{PM} = 1.6 \cdot 10^{-3} \text{ ergs-cm}^{-2}\text{-s}^{-1} \qquad (4.14)$$

These results show that energy lost by wave breaking and contributing to turbulence depends on the spectral shape which in turn depends on the state of the sea. It appears that generation of near surface turbulence by breaking waves is more important for increasing wind speeds when seas are growing than for constant or decreasing wind speeds when seas tend to be near full development. This behavior is consistent with visual wave observations which indicate increased wave breaking for increasing wind speeds.

A comparison of the energy flux from breaking waves to the energy flux to surface currents from the wind is useful. The power, or rate at which energy (here, per unit area), is transferred from the wind into surface currents is given by the wind stress multiplied by the wind friction velocity or the wind stress multiplied by an approximate surface current speed. The friction velocity, u*, is related to the wind speed by $u^* = (C_D)^{1/2} u$ where C_D is the drag coefficient in the relationship

$$\tau = \rho_{air} C_D u^2 \qquad (4.15)$$

For $C_D = 1.5 \cdot 10^{-3}$, an often used value, the energy flux $\dot{E}$ from wind to currents is given by

$$\dot{E}_{current} = \tau u^* = \rho_{air} C_D^{3/2} u^3 = \rho_{air} u^{*3} = 7.6 \cdot 10^{-8} u^3 \qquad (4.16)$$

An approximate surface current speed can be estimated from

$$\rho_{air} C_D u^2 = \rho_{water} C_D u_{water}^2 \quad \text{or} \quad u_{water} \simeq 0.035u \qquad (4.17)$$

which is almost the same as $u^* = 0.039u$ obtained for $C_D = 1.5\ 10^{-3}$. Division of Equation (4.11), the energy flux from breaking waves for an equilibrium spectrum, by Equation (4.16), the energy flux from the wind shows that

$$\frac{\text{Energy flux from waves}}{\text{Energy flux from wind}} \simeq 1/3 \quad \text{(equilibrium spectrum)} \qquad (4.18)$$

In other words, the energy flux from breaking waves may be an appreciable portion of the energy flux from the wind. However, for a Pierson-Moskowitz spectrum

$$\frac{\text{Energy flux from waves}}{\text{Energy flux from wind}} \simeq 2.1 \cdot 10^{-5} \simeq 0 \quad \text{(Pierson-Moskowitz spectrum)} \qquad (4.19)$$

Thus, the importance of wave breaking as a function of wind speed depends on the spectral shape and the state of the sea. Because wave spectra can have a wide variety of shapes, including multiple peaks when both sea and swell are present, dependence on spectral shape indicates that these calculations should be considered as qualitatively, rather than quantitatively, indicating the importance of wave breaking.

During wave breaking in deep water, amplitudes of breaking waves are reduced below values determined by wave breaking criteria. The energy from the waves is lost very near the sea surface and not over the total depth, approximately one-half a wave length, for which wave orbital velocities are non-negligible. Turbulence is essentially injected near the sea surface. Thompson (1982) has used this concept to develop a potential flow model of breaking wave turbulence which shows that the turbulent kinetic energy decreases in proportion to the inverse square of the depth. Hence, turbulent velocity fluctuations decrease inversely with depth. Regardless of the exact depth variation of the turbulence, the magnitude of the energy flux from breaking waves indicates potential for substantial mixing and turbulence near the surface. In the very near surface region less than a few surface wave amplitudes from the surface, decreased vertical gradients of current velocity and other parameters would be expected.

C. MAINTENANCE OF TURBULENCE

The velocity shear of Stokes currents may be a mechanism for waves to maintain turbulence within the upper ocean. The rate of depth attenuation of Stokes currents permits such a mechanism to extend to depths comparable to those of seasonal thermoclines. If waves contribute to the maintenance of turbulence within the upper ocean, the associated increased eddy viscosity (and eddy coefficients for other parameters) due to the waves would result in decreased current shear (and vertical

gradients of other properties). That is, a surface layer would be better mixed than it would be for similar conditions but without waves. Maintenance of turbulence by waves requires a wave-induced velocity shear. Wave orbital velocities have no shear when averaged over time. However, as suggested by Phillips (1961) and also explained by Longuet-Higgins (1968), the mean velocity shear associated with Stokes currents can contribute to the maintenance of turbulence. The derivation involves a balance between the dissipation of vorticity by viscosity and criterion of vorticity through Stokes current shear. The root-mean-square value of vorticity is found to be

$$(\overline{\omega^2})^{\frac{1}{2}} \simeq (ak)^2 \sigma \exp(2kz) \tag{4.20}$$

which decreases exponentially with depth as Stokes currents do. Use of 1/k as a characteristic length scale yields turbulent velocity fluctuations, v'_t, possibly as large as

$$v'_t \simeq \frac{(\overline{\omega^2})^{\frac{1}{2}}}{k} = (ak)(a\sigma)\exp(2kz) \tag{4.21}$$

As noted by Longuet-Higgins (1968), the ratio of turbulent kinetic energy to wave kinetic energy is $(ak)^2$. This occurs because wave energy is proportional to $(a\sigma)^2$ and turbulent energy is proportional to $(v'_t)^2$. For typical wave slopes, ak = 0.1, this ratio is 0.01 = 1%, indicating the great practical difficulty in measuring wave-caused turbulence. However, the ratio may reach approximately 25% for high steep waves near breaking when ak is near 0.5.

Equation (4.21) can be used to give a rough estimate of the eddy viscosity, K_M, which is related to the turbulent velocity fluctuations, u' and w', in the horizontal and vertical directions by

$$\overline{u'w'} = - K_M \frac{\partial u}{\partial z} \tag{4.22}$$

where $\partial u/\partial z$ is vertical shear. If this shear is due to a Stokes current, $(v'_t)^2$ approximates u'w' so that

$$K_M \simeq \frac{a^2\sigma}{2} \exp(2kz) \tag{4.23}$$

The derivations resulting in the K_M estimate are implicity for the interior of the upper ocean so that large values of K_M as z approaches zero in Equation (4.23) may not be realistic. Integration of Equation (4.23) over a depth, here taken as one-half a wave length, below which wave motion is negligible provides a single rough estimate of K_M for quantitative evaluation. The average value of K_M over this depth is found to be

$$\langle K_M \rangle_1 \simeq a^2\sigma/(4\pi) \tag{4.24}$$

If the sea surface is treated as a boundary so that K_M is given by

$$K_M = k_o w^* z \tag{4.25}$$

where k_o is Von Karmen's constant (0.4) and if w^* is approximated by v'_t, a reduced average value of K_M is found to be

$$\langle K_M \rangle_2 \simeq k_o a^2\sigma/(4\pi) \tag{4.26}$$

For growing waves, an interesting observation is that a^2 increases approxmately as the fourth power of the wind speed and σ decreases approximately inversely with wind speed so that $\langle K_M \rangle$ increases with the cube of the wind speed. Thus, $\langle K_M \rangle$ has the same wind speed dependence as the energy lost from wave breaking. The increase of $\langle K_M \rangle$ indicated here also shows that K_M may be underestimated and vertical shear may be overestimated in some current shear models. Some models use a constant eddy viscosity which does not increase with wind speed. Also, if it is assumed that the energy flux from the wind to the currents ($\rho_{air} u^{*3}$ as earlier noted) is dissipated within the mixed layer, the eddy viscosity in the mixed layer is proportional to the wind speed. At lower wind speeds, the dependence of K_M on wind speed may not be critical. However, at higher wind speeds such as those which occur fairly often during extratropical storms at mid-latitudes to high latitudes, dependence of K_M on a high power of wind speed would substantially decrease near surface vertical shear.

A few numerical examples for $\langle K_M \rangle$ are of interest. For a wave amplitude, a = 100 cm, and a wave period of 10 sec (σ = 0.628),

$$\langle K_M \rangle_1 \simeq 500 \text{ cm}^2\text{-s}^{-1}$$

$$\langle K_M \rangle_2 \simeq 200 \text{ cm}^2\text{-s}^{-1} \qquad (4.27)$$

Instead of considering a single surface wave, an equilibrium spectrum defined by Equation (4.6) can be used to examine wind speed dependence. The zero-crossing frequency, as

given in Equation (4.5), can be used for σ and the root-mean-square wave amplitude can be used for a. The root-mean-square wave amplitude is given by

$$2^{\frac{1}{2}} \int_0^{\infty} E(\sigma)\, d\sigma \tag{4.28}$$

The results are

$$\langle K_M \rangle_1 \simeq \frac{\alpha u^3}{2^{5/2}\pi g} = 7.1 \cdot 10^{-7} u^3 \tag{4.29}$$

$$\langle K_M \rangle_2 \simeq \frac{k_o \alpha u^3}{2^{5/2}\pi g} = 2.8 \cdot 10^{-7} u^3 \tag{4.30}$$

where cgs units are used. These results can be compared to a wind dependent eddy viscosity (Neumann and Pierson, 1966) that is sometimes used

$$K_{M_3} = 1.8 \cdot 10^{-5} u^{2.5} \tag{4.31}$$

Table 4.1 lists values of $\langle K_M \rangle_1$, $\langle K_M \rangle_2$, and K_{M3} as a function of wind speed. While the values in Table 4.1 are rough and may be correct only in a general comparative sense, it is concluded that maintenance of turbulence by waves can be related to sufficiently high eddy viscosity values to substantially reduce vertical shear. Shear models employing a constant eddy viscosity or an eddy viscosity that increases linearly with wind speed cannot match the behavior shown in Table 4.1 and could over-estimate shear at higher wind speeds.

If waves help to maintain turbulence and to increase eddy viscosity values, there

TABLE 4.1.

Comparison of Eddy Viscosity Values (cm^2-s^{-1}) as Functions of Wind Speed.

u(cm-s^{-1})	u[1](knots)	$\langle K_M \rangle_1$	$\langle K_M \rangle_2$	K_{M3}
500	10	89	39	100
1000	20	710	280	569
1500	30	2,396	945	1,569
2000	40	5,680	2,240	3,220
2500	50	11,094	4,375	5,620

[1]approximate

would be a similar increase in values of turbulent eddy coefficients for other parameters such as heat, salt, and chemical properties. For example, if the upper ocean is well enough mixed, the eddy coefficient, K_T, for heat would be about of the same magnitude as K_M so that K_T would change with surface wave conditions in a manner similar to K_M. Increased eddy coefficients due to surface waves would result in a better mixed surface layer. As an example, the flux of heat through the upper ocean is given by $-K_T \partial T/\partial z$ where T is temperature. When the heat flux through the sea surface varies slowly in comparison to changing wave conditions, a wave caused increase in K_T results in a reduced temperature gradient. This behavior can be modelled for the time varying case by numerically solving the heat conduction equation with a time varying (and potentially depth varying) eddy coefficient dependent on surface wave conditions. The results may be different than similar solutions in which eddy coefficients vary with wind speed. This occurs because wave conditions depend on other factors (such as wind fetch and duration) than wind speed and swell is not a function of local wind speed.

D. VERIFICATION BY MEASUREMENTS

Effects of wave breaking and of wave maintenance of turbulence have not been quantified by interpretation of measurements. Shallow water measurements and tank tests have limitations because of bottom effects on wave breaking and boundary effects on turbulence. There have been several significant problems in making appropriate measurements in the open ocean. These problems include: lack of fixed platforms for sensor attachment with resultant introduction of sensor motion induced errors, importance of the surface effects for high wave conditions when measurements are most difficult, and difficulty in separating non-wave motion (i.e. turbulence) from the much larger wave motion when measurement errors, sampling variability of wave statistics, and non-linear wave theories are considered.

From a modeling approach, surface waves cause increased eddy coefficient values so that wave effects may be implicitly and partly included in models in which eddy coefficients vary with wind speed. Davis et al. (1981b) interpret the MILE measurements described by Davis et al. (1981a) by means of an empirical model based on the parameter, ρu^{*3}, which is used earlier in this section. Since it is shown that the rate of energy loss from wave breaking and eddy coefficients due to wave maintenance of turbulence are proportional to wind speed cubed, which is proportional to u^{*3}, the work of Davis et al. may implicitly include surface wave effects. Of interest is the fact that the strong wind speed dependence of wave effects would contribute to increased mixing during high wind events leading to slab-like low shear flow of the upper layer as described by Davis et al. (1981a,1981b). Discrepancies between model results of Davis et al. (1981b) and the observations, such as differences between calculated and observed transport and temporal deviations of model results from measurements, might be due to the role of surface waves as an intermediary between winds and currents. Since wave conditions are not just a function of wind speed, parameterizations involving only wind speed may not be able to fully represent vertical structure and temporal variations of the upper ocean.

5. REGIONS OF GEOGRAPHICAL IMPORTANCE

The previous sections note that surface wave effects of interest are mainly second order effects in terms of wave theory and that these effects increase with sea state. These effects are more important in regions with higher wind speeds than in regions with lower wind speeds. Dependence of each effect on wind speed is noted in the previous sections. The best manner by which to examine wave effects for various geographical regions would be to develop statistical probability distributions of effect magnitudes based on wave climatology statistical probability distributions. However, the theories include simplifying assumptions and have not been verified by ocean measurements. Also, surface wave directional spectra should be considered in such an approach. These points are further discussed in following sections. For the purpose of providing a general description of regions where these effects would be of most importance, examination of the dependence of these effects on wind speed is adequate. Following is a summary of this dependence where u is wind speed:

-- Magnitude of surface wave generated inertial currents - proportional to u,

-- Growth rate of internal wave amplitudes calculated from surface wave spectra - proportional to $u^{3.5}$,

-- Rate of energy loss due to wave breaking - proportional to u^3, and

-- Eddy viscosity due to wave maintenance of turbulence - proportional to u^3.

These statements of proportion are for general comparison purposes only. Derivations

providing these results are in previous sections and show that other factors besides just wind speed are involved. The wind speed exponents can also be changed by making different theoretical assumptions, for example by using different surface wave spectra formulations.

Wind speed dependence shows that the mid-to-high latitude regions of interest to the OMP are regions where surface wave effects are most likely important. These regions include primary extratropical storm tracks and are regions where high wind speeds are relatively frequent. During winter, speeds are often higher than those during most upper ocean measurement experiments so that surface wave effects that may be important operationally may not be detected in these experiments. Since higher wind speeds associated with storms are intermittent at a given location depending on when storms pass nearby, surface wave effects are also expected to be intermittent phenomena with time varying degrees of importance. Wind speed dependence also indicates a strong seasonal variation of the importance of surface wave effects. For the generation of internal waves through interaction with surface waves, seasonal variation is a combined function of wave conditions and characteristics of the seasonal thermocline.

6. ADDITIONAL DATA REQUIREMENTS

Based on the previous sections, the following wave effects are judged to be potentially significant for the OMP.

-- Generation of inertial currents and associated vertical shear,

-- Generation of high frequency internal waves within the seasonal thermocline, and

-- Increased mixing and decreased vertical gradients near the surface due to wave breaking and wave maintenance of turbulence.

No open ocean measurements have been interpreted in a manner to quantitatively determine the importance of these effects. Without such measurment interpretation, no theoretical or modeling technique can be judged suitable for routine operational use. For applications of interest to the OMP, the most information would be gained from field measurements and data analysis to more quantitatively evaluate wave effects. As examples, the measurements of inertial currents described by Rubenstein and Newman (1982), of internal waves described by Kase and Clarke (1978), and of upper ocean variability in the MILE experiment (Davis et al., 1981a, 1981b; Dillon and Caldwell, 1980) perhaps could be interpreted somewhat differently if wave effects are considered. However, for such past measurments there may be poor surface wave information, particularly measurements, to aid such interpretations. Planning of future OMP field experiments to collect supplemental surface wave data is a feasible approach to develop needed data sets. The remainder of this section provides guidelines for such planning.

Analysis of upper ocean measurement with the goal of identification of surface

wave effects requires the following information:

-- Simultaneous surface wave and upper ocean measurements for a variety of sea states, especially some high sea states,

-- Knowledge of surface wave directional spectra and spectra variations over time periods of at least several days corresponding to time periods over which meteorological forcing variations occur,

-- Upper ocean measurements of vertical shear, inertial currents, internal waves within and above the seasonal thermocline, and density stratification over the same time periods,

-- Continuous (i.e. suitable for time averaging) and accurate (i.e. not standard bridge observations) measurements of local wind velocity over the same time periods, and

-- Synoptic meteorological information, primarily from analysis of weather charts, over a large area potentially as large as the ocean of interest.

In addition, incorporation of surface wave hindcast information into the analysis would be advantageous for two reasons. First, surface wave directional spectra can be determined more accurately from hindcasts than from deep ocean measurements in higher sea states. Second, there are existing hindcasts covering sufficient years in both the North Atlantic and North Pacific Oceans to develop a directional wave spectra climatology as a function of location on a seasonal or monthly basis. Analysis of upper ocean data for wave effects possibly would reveal empirical relationships, such as mathematical

parameterizations, between these effects and hindcast surface wave spectra. A surface wave spectra climatology could then be used with these relationships to prepare a climatological description of surface wave effects. Thus, such a description might be available before development and verification of more complex theoretical and/or numerical modeling techniques.

The two approaches for determination of surface wave information are to make surface wave measurements simultaneously with other upper ocean measurements and to hindcast wave conditions at times and locations of the upper ocean measurements. By themselves, both approaches have limitations. There is not a routine operational method to measure surface wave directional spectra with good directional resolution. For example, a pitch-roll-heave buoy typically provides a directional resolution of between 88° and 130° depending on the type of data processing. Directional spectra from such a buoy almost always have a broad directional width. To obtain significantly better directional resolution, an array of sensors is needed and use of such an array is not practical in deep water, particularly during high wave conditons. There is much literature on measurement of surface wave directional spectra (e.g. reviews by Panicker, 1974, and Borgman, 1979) but it is not appropriate to discuss measurement details here. Rather than being measured in-situ, directional spectra can be remotely sensed by various types of radar sensors on aircraft or satellites. Such techniques are considered still in the research phase and instrumention of additional aircraft for Naval use in deep ocean areas potentially far from coasts would be a major and expensive effort. For the foreseeable future, the best approach is to determine surface wave non-directional spectra from measurements of wave elevation only as a function of time. Several commercially made sensors, such as widely used Waverider buoys, are available and are capable of making measurements in high sea states. However, calibration of commercially available sensors is critical. For example, Baer et al. (1981) and Ribe (1982) show that use of uncalibrated

Waverider buoys may result in wave amplitude errors as large as 10% to 15%. Because the surface wave effects considered here are proportional to powers of wave amplitude, such errors would be amplified. With only measurement of surface wave non-directional spectra, wave directional characteristics could be inferred from synoptic weather charts, actually from wind fields calculated from these charts, or by means of wave hindcasts. Use of a numerical surface wave directional spectra model in hindcast mode is the more complex but better approach. Use of wave hindcasts by themselves does not permit evaluation of uncertainties associated with wind fields that are input into the wave model or of the model itself. Calibration of hindcasts with the non-directional measurements helps decrease uncertainties.

Several numerical surface wave directional spectra models are adequate for hindcast use after a field experiment. While preparation of input wind fields and model implemetation requires time, further model development does not seem necessary for the purposes of the OMP. Among available models are the U.S. Navy Spectral Ocean Wave Model, SOWM, (e.g. Pierson, 1982), the U.S. Army Corps of Engineers Wave Information Study Model (e.g. Corson et al., 1981), and a model that has been set-up globally (Earle et al., 1982). Several publications (e.g. Favre and Hasselmann, 1978; Cardone, 1979; Earle, 1981) review numerical wave models and a review is not needed here. For the purpose of initially analyzing upper ocean measurements for surface wave effects, the choice of a particular state-of-the-art model is probably not critical. Of most importance is probably capability to implement and use a state-of-the-art model relatively rapidly and at reasonable cost.

The SOWM model has been used for a twenty year hindcast covering the North Atlantic and North Pacific Oceans. NOAA's National Climatic Center has just completed a geographical sort of the many data tapes from this hindcast. Thus, it is possible to

develop surface wave directional spectra climatologies at locations of interest without reading all data tapes from the hindcast. The U.S. Army Corps of Engineers model has been used for a twenty year hindcast covering the North Atlantic Ocean. Hard copy summaries of results are available for U.S. coastal and continental shelf locations and the Corps will later be able to provide additional results in a data base. These two existing hindcasts would not be of use for a future upper ocean field experiment, but they would be useful for climatological evaluations. Additional assessments of accuracies of existing hindcasts should be part of such a climatological study. In the wave modeling community, there is a range of opinion about the accuracies of these hindcasts.

Capability to make the internal upper ocean measurements has been and is being developed by the OIS part of the OMP. For determination of surface wave effects, it is necessary to make upper ocean measurements simultaneously with wave measurements.

Suitable measurement of wind velocity is not difficult but wind measurements should be nearly continuous with a relatively small sampling and/or averaging interval on the order of seconds to a few minutes. Calculations of time-averaged wind velocities and stresses to drive both current and surface wave models and to interpret upper ocean measurements are sensitive to the averaging period and capability to use different averaging periods in the analysis may be needed.

Synoptic weather information, mainly weather charts, can be obtained from the Navy and NOAA's National Meteorological center. Accurate development of wind fields from such charts requires considerable effort. During such development, supplemental use of all available ship observations obtained from the U.S. Navy Fleet Numerical Oceanographic Center and NOAA's National Climatic Center is desirable.

Overall, development of dats sets to quantitatively evaluate surface wave effects as part of future OMP field experiments does not present unusually difficult problems. Measurement of surface wave directional spectra with good directional resolution is not routinely possible but development of such wave-specific instrumentation is a major effort and is probably not justified solely for OMP applications. With measurement of non-directional wave spectra for verification of surface wave hindcasts, surface wave directional information can be obtained from hindcasts. Since internal upper ocean measurements will be made by the OMP in any case, development of needed surface wave information could be a supplemental effort accompanying the other measurements.

7. SUMMARY

Three types of surface wave effects are potentially important to the OMP. These are:

-- Generation of inertial currents and associated vertical shear,

-- Generation of high frequency internal waves within the seasonal thermocline, and

-- Increased mixing and decreased vertical gradients near the surface due to wave breaking and wave maintenance of turbulence.

Theory relating to each of these effects is provided and mathematical calculations are made which indicate the potential importance of these effects for the OMP. These effects increase with wind speed and sea state and are thus potentially important in mid-to-high latitude regions. These regions have relatively high wind speeds and wave heights due to prevailing westerly winds and the presence of primary extratropical storm tracks. Surface wave effects are largest near the surface and may be significant for depths less than approximately 100 meters.

No measurements have been previously interpreted in a manner to quantitatively determine the importance of surface wave effects in the actual ocean. Such interpretation is needed because these effects are second order effects in terms of wave theory and existing theoretical approaches involve simplifying assumptions. Without suitable data interpretation, no theoretical or modeling technique can be judged suitable for routine operational use. Wave effects may be implicitly, but incorrectly, considered in present upper ocean models and data interpretations with wind dependence. This

situation occurs because surface wave effects increase with sea state which increases with wind speed. However, the intermediate role of waves between the wind and upper ocean features changes the form of wind speed dependence so that improved results might be obtained by consideration of wave effects. Characteristics of several existing upper ocean data sets are consistent with the presence of surface wave effects and consideration of wave effects might lead to different interpretations than have been reported for these data sets. A shortcoming of existing data sets is that the measurements were not planned to evaluate surface wave effects so that information for detailed analysis may not be available.

Since the importance of surface wave effects has not been proven from measurements, emphasis should be placed on supplemental development of wave information, including measurements and hindcasts, during future upper ocean field experiments to provide data sets suitable for further analysis of wave effects. Guidance is provided for development of needed wave information.

8. BIBLIOGRAPHY

Apel, J.R., H.M. Byrne, J. R. Proni, and R.L. Charnell, Observations of Oceanic Internal and Surface Waves from the Earth Resources Technology Satellite, Journal of Geophysical Research, 80, 865-881, 1975.

Baer, L., An Experiment in Numerical Forecasting of Deep Water Ocean Waves, Report LMSC-801296, Lockheed Missile and Space Company, San Diego, Calif., 1962.

Baer, L., D. Esteva, L. Huff, W. Iseley, R. Ribe, and M.D. Earle, Some Problems in the Development of the National Coastal Waves program, Proceedings of the Symposium on Wave Dynamics and Radio Probing of the Ocean Surface, Miami, 1981, in press, 1983.

Ball, F.K., Energy Transfer Between External and Internal Gravity Waves, Journal of Fluid Mechanics, 19, 465-480, 1964.

Bishop, J.M., A Note on Surface Wind-driven Flow, Ocean Engineering, 6, 273-284, 1979.

Borgman, L.E., Directional Wave Spectra from Wave Sensors, Ocean Wave Climate, M.D. Earle and A. Malahoff (eds.), Plenum Press, N.Y., 269-300, 1979.

Brekhovskikh, LM., V.V. Goncharov, V.M. Kurtepov, and K.A. Nangol'nykh, Resonant Excitiation of Internal Waves by Nonlinear Interaction of Surface Waves, Izv. Akad. Nauk. SSSR Fiz. Atmos. Okeana, 8, 192-203, 1972. (Izv. Acad. Sci. USSR Atmos. Oceanic Phys., 8, Engl. Transl., 112-117, 1972.)

Bye, J.A.T., The Wave-drift Current, Journal of Marine Research, 25, 95-102, 1967.

Cardone, V.J. and D.B. Ross: "State-of-the-Art Wave Prediction Methods and Data Requirements," in: Ocean Wave Climate, M.D. Earle and A. Malahoff (eds.), Plenum Press, N.Y., 61-91, 1979.

Chang, M.S., Mass Transport in Deep Water Long Crested Random Gravity Waves, Journal of Geophysical Research, 74, 1515-1536, 1969.

Chin, H., An Evaluation of Stokes Velocities and Inertial Currents Generated by Deep-water Surface Gravity Waves, New York University Geophys. Sci. Lab. Report, 71-11, 1971.

Corson, W.D., D.T. Resio, R.M. Brooks, B.A. Ebersole, R.E. Jensen, D.S. Rassdale, and B.A. Tracy, Atlantic Coast hindcast, Deepwater, Significant Wave Information, U.S. Army Engineer Waterways Experiment Station, Hydraulics Laboratory, Vicksburg, MS. Report No. WIS-2, 15 pp., 1981.

Craik, A.D. and S. Leibovich, A Rotational Model for Langmuir Circulations, Journal of Fluid Mechanics, 73, 401-426, 1976.

Davis, R.E., R. DeSzoeke, D. Halpern, and P. Niiler, Variability in the Upper Ocean During MILE, Part I: the Heat and Momentum Balances, Deep Sea Research, 28A, 1427-1451, 1981a.

Davis, R.E., R. DeSzoeke, and P. Niiler, Variability in the Upper Ocean During MILE, Part II: Modeling the Mixed Layer Response, Deep Sea Research, 28A, 1453-1475, 1981b.

Dillon, T.M. and D.R. Caldwell, High-Frequency Internal Waves at Ocean Station P, Journal of Geophysical Research, 85, 3277-3284, 1980.

Earle, M.D., Problems in Ocean Wave Hindcasting, in: Spaceborne Synthetic Aperture Radar for Oceanography, R.C. Beal, P.S. DeLeonibus, and I. Katz (eds.), Johns Hopkins University Press, Baltimore, MD, 1981.

Earle, M.D., K.A. Bush, J.M. Bishop, and E.E. Lacour, Development of a Global Ocean Swell Model, Offshore Technology Conference Paper 4327, 1982.

Ekman, V.M., On the Influence of the Earth's Rotation on Ocean Currents, Ark. Mat. Astr. Fys., 2, 1-55, 1905.

Favre, A. and K. Hasselmann (eds.), Turbulent Fluxes Through the Sea Surface, Wave Dynamics and Prediction, Plenum Press, NY, 1978.

Goodman, L., and E.R. Levine, Generation of Oceanic Internal Waves by Advecting Atmospheric Fields, Journal of Geophysical Research, 82, 1711-1717, 1977.

Hasselmann, K.A., Feynman Diagrams and Interaction Rules of Wave-Wave Scattering Processes, Reviews of Geophysics, 4, 1-32, 1966.

Hasselmann, K., Wave-driven Inertial Oscillations, Geophysical Fluid Dynamics, 1, 463-502, 1970.

Huang, N.E., On Surface Drift Currents in the Ocean, Journal of Fluid Mechanics, 91, 191-208, 1979.

Huang, N.E., An Oilspill Trajectory Analysis Model with a Variable Wind Deflection Angle, Ocean Engineering, in press, 1982.

Ianniello, J.P., and R. Garvine, Stokes Transport by Gravity Waves for Application in Circulation Models, Journal of Geophysical Research, 5, 47-50, 1975.

Joyce, T.M., Nonlinear Interactions Among Standing Surface and Internal Gravity Waves, Ph.D. Dissertation, Massachusetts Institute of Technology, Report 72-3, 1972.

Joyce, T.M., Nonlinear Interactions Among Standing Surface and Internal Gravity Waves, Journal of Fluid Mechanics, 63, 801-825, 1974.

Kase, R.H., and R.A. Clarke, High Frequency Internal Waves in the Upper Thermocline During GATE, Deep Sea Research, 25, 815-825, 1978.

Kenyon, K.E., Wave-Wave Interactions of Surface and Internal Waves, Journal of Marine Research, 26, 208-231, 1968.

Kenyon, K.E., Stokes Drift for Random Gravity Waves, Journal of Geophysical Research, 74, 6991-6994, 1969.

Kenyon, K.E., Stokes Transport, Journal of Geophysical Research, 75, 1133-1135, 1970.

Kirwan, A.D., Jr., G. McNally, S. Pazan, and R. Wert, Analysis of Surface Current Response to Wind, Journal of Physical Oceanography, 9, 401-412, 1979.

Korvin-Krovkovsky, B.V., Pure Drift Current and Mass Transport in Coexistent Waves, Deut. Hydro. 2, 25, 1-13, 1972.

Leibovich, S., On the Evolution of the System of Wind Drift Currents and Langmuir Circulations in the Ocean, Part 1, Theory and Average Current, Journal of Fluid Mechanics, 79, 715-743, 1977.

Longuet-Higgins, M.S., On the Generation of Turbulence by Wave Motions, Notes for the Symposium on Turbulence in the Ocean, University of British Columbia, Vancouver, British Columbia, Canada, 1968.

Longuet-Higgins, M.S., On the Transport of Mass by Time-varying Ocean Currents, Deep Sea Res., 16, 431-447, 1969.

Longuet-Higgins, M.S., On Wave Breaking and the Equilibrium Spectrum of Wind-Generated Waves, Proceedings of the Royal Society, A, 310, 151-159, 1969.

Madsen, O.S., Mass Transport in Deep-water Waves, Journal of Physical Oceanography, 8, 1009-1015, 1978.

Naval Weather Service Detachment, U.S. Navy Marine Climatic Atlas of the World, Volume 1, North Atlantic Ocean, 1974.

Nesterov, S.V., Resonant Interaction of Surface and Internal Waves, Izv. Acad. Sci. USSR Atmos. Oceanic Phys., 8, 252-254, 1972.

Neumann, G. and W.J. Pierson, Principles of Physical Oceanography, Prentice Hall, Englewood Cliffs, N.J., 1966.

Olbers, D.J., and K. Herterich, The Spectral Energy Transfer from Surface Waves to Internal Waves, Journal of Fluid Mechanics, 92, 349-379, 1979.

Panicker, N.N., Review of Techniques for Directional Wave Spectra, Proceedings of the International Symposium on Ocean Wave Measurement and Analysis, New Orleans, LA, American Society of Civil Engineers, 669-688, 1974.

Phillips, O.M., A Note on the Turbulence Generated by Gravity Waves, Journal of Geophysical Research, 66, 2889-2893, 1961.

Phillips, O.M., The Dynamics of the Upper Ocean, Cambridge University Press, New York, N.Y., second edition, 1977.

Pierson, W.J., L.J. Tick and L. Baer, Computer Based Procedures for Preparing Global Wave Forecasts and Wind Field Analyses Capable of USing Wave Data Obtained by a Spacecraft, Sixth Naval Hydrodynamics Symposium, Office of Naval Research, Washington, D.C., 499-532, 1966.

Pierson, W.J. and L. Moskowitz, A Proposed Spectral Form for Fully Developed Wind Seas Based on the Similarity Theory of S.A. Kitaigorodskii, Journal of Geophysical Research 69, 5181-5190, 1964.

Pierson, W.J., The Spectral Ocean Wave Model, SOWM, A Northern Hemisphere Computer Model for Forecasting Ocean Wave Spectra, David W. Taylor Naval Ship Research and Development Center, July, 1982.

Pollard, R.T., and R. Millard, Comparison between Observed and Simulated Wind-generated Inertial Oscillations, Deep-Sea Research, 17, 813-821, 1970.

Ribe, R.L., Calibrations and Energy Spectrum Corrections for Waverider Buoys Deployed Under the ARSLOE Program, NOAA Ocean Technology and Engineering Services Technical Report, 1982.

Roth, M.W., M.G. Briscoe, and C.H. McComas III, Internal Waves in the Upper Ocean, Journal of Physical Oceanography, 11, 1234-1247, 1981.

Rubenstein, D.M., A Model of Vertical Dispersion of Inertial Waves in the Upper Ocean, Science Applications Inc. Report SAI-83-861-WA, for Ocean Measurements Program, Naval Ocean Research and Development Activity, NSTL Station, Mississippi, 1982.

Rubenstein, D.M., and F.C. Newman, Analysis of Shear from Ocean Current Meters, Science Applications Inc. Report SAI-82-687-WA, for Ocean Measurements Program, Naval Ocean Research and Development Activity, NSTL Station, Mississippi, 1982.

Stokes. G.G., On the Theory of Oscillatory Waves, Transactions of the Cambridge Philosophical Society, 8, 441-455, 1847.

Thompson, R.O.R.Y., A Potential Flow Model of Turbulence Caused by Breaking Surface Waves, Journal of Geophysical Research, 87, 1935-1937, 1982.

Thorpe, S.A., On Wave Interactions in a Stratified Fluid, Journal of Fluid Mechanics, 24, 737-751, 1966.

Thorpe, S.A., The Excitation, Dissipation, and Interaction of Internal Waves in the Deep Ocean, Journal of Geophysical Research, 80, 328-338, 1975.

Ursell, Fl, On the Theoretical Form of Ocean Swell on a Rotating Earth, Mon. Nat. R. Astr. Soc. Geophys. Suppl., 6, 1-6, 1950.

Watson, K.M., B.J. West, and B.I. Cohen, Coupling of Surface and Internal Gravity Waves: A Mode Coupling Model, Journal of Fluid Mechanics, 77, 185-208, 1976.